
WHALE: TOWARDS GENERALIZABLE AND SCALABLE WORLD MODELS FOR EMBODIED DECISION-MAKING

Zhilong Zhang^{1,2,3*}, Ruifeng Chen^{1,2,3*}, Junyin Ye^{1,2,3*}, Yihao Sun^{1,2}, Pengyuan Wang^{1,2,3},
Jingcheng Pang^{1,2,3}, Kaiyuan Li^{1,2,3}, Tianshuo Liu^{1,2,3}, Haoxin Lin^{1,2,3},
Yang Yu^{1,2,3†}, Zhi-Hua Zhou^{1,2}

¹National Key Laboratory for Novel Software Technology, Nanjing University, Nanjing, China

²School of Artificial Intelligence, Nanjing University, Nanjing, China

³Polixir Technologies, Nanjing, China

{zhangzl, chenrf, yejy, sunyh, wangpy, pangjc, liky, liuts, linhx}@lamda.nju.edu.cn,
{yuy, zhouzh}@nju.edu.cn

ABSTRACT

World models play a crucial role in decision-making within embodied environments, enabling cost-free explorations that would otherwise be expensive in the real world. To facilitate effective decision-making, world models must be equipped with strong **generalizability** to support faithful imagination in out-of-distribution (OOD) regions and provide reliable **uncertainty estimation** to assess the credibility of the simulated experiences, both of which present significant challenges for prior scalable approaches. This paper introduces WHALE, a framework for learning generalizable world models, consisting of two key techniques: *behavior-conditioning* and *retracing-rollout*. Behavior-conditioning addresses the policy distribution shift, one of the primary sources of the world model generalization error, while retracing-rollout enables efficient uncertainty estimation without the necessity of model ensembles. These techniques are universal and can be combined with any neural network architecture for world model learning. Incorporating these two techniques, we present Whale-ST, a scalable spatial-temporal transformer-based world model with enhanced generalizability. We demonstrate the superiority of Whale-ST in simulation tasks by evaluating both value estimation accuracy and video generation fidelity. Additionally, we examine the effectiveness of our uncertainty estimation technique, which enhances model-based policy optimization in fully offline scenarios. Furthermore, we propose Whale-X, a 414M parameter world model trained on 970K trajectories from Open X-Embodiment datasets. We show that Whale-X exhibits promising scalability and strong generalizability in real-world manipulation scenarios using minimal demonstrations.

1 Introduction

Human beings can envision an imagined world in their minds, predicting how different actions might lead to different outcomes [1, 2]. Inspired by this aspect of human intelligence, world models [3] are designed to abstract real-world dynamics and provide such “*what if*” prediction. As a result, embodied agents can interact with world models instead of real-world environments to generate simulation data, which can be used for various downstream tasks, including counterfactual prediction [4], off-policy evaluation [5], and offline reinforcement learning [6]. The requirement to facilitate more effective decision-making presents substantial challenges to the generalizability of world models, an issue that previous approaches have not adequately addressed [7]. Additionally, achieving reliable uncertainty estimation for imagined visual experiences remains a significant challenge, impacting the trustworthy utilization of synthetic data in offline policy optimization [8]. These two unresolved issues impede the further success of world models in supporting decision-making.

*Equal Contribution

†Corresponding Author

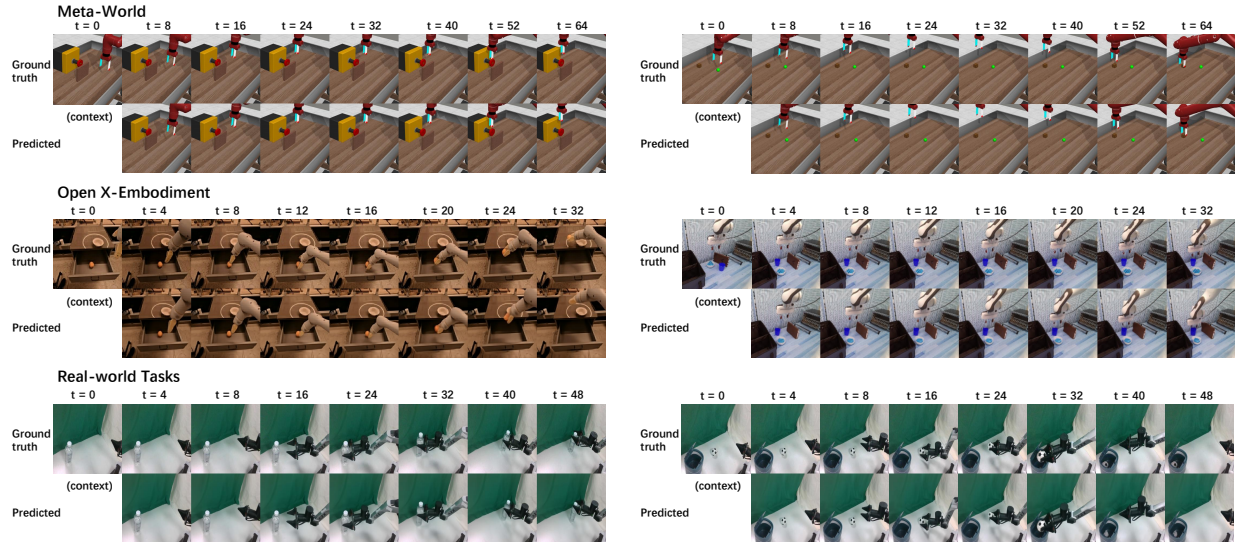


Figure 1: Qualitative evaluation on Meta-World, Open X-Embodiment, and our real-world tasks.

In this work, we introduce WHALE (World models with beHavior-conditioning and retrAcing-rollout LEarning), a framework for learning generalizable world models, consisting of two key techniques that can be universally combined with any neural network architecture. First, based on the identification of policy distribution divergence as a primary source of the generalization error, we introduce a **behavior-conditioning** technique to enhance the generalizability of world models, which builds upon the concept of policy-conditioned model learning [9] aiming to enable the model to adapt to different behaviors actively to mitigate the extrapolation error caused by distribution shift. Furthermore, we propose a simple yet effective technique called **retracing-rollout**, to enable efficient uncertainty estimation for the model imagination. This approach avoids the necessity of computation-expensive ensembles of the visual world models while providing a reliable uncertainty estimation to facilitate policy optimization in fully offline scenarios. As a plug-and-play solution, the retracing rollout can be efficiently applied to end-effector pose control in various embodiment tasks without necessitating any changes to the training process.

To implement the WHALE framework, we present Whale-ST, a scalable embodied world model based on the spatial-temporal transformer [10, 11], designed to enable faithful long-horizon imagination for real-world visual control tasks. To substantiate the effectiveness of Whale-ST, we conduct extensive experiments on both simulated Meta-World [12] benchmark and a physical robot platform, encompassing a variety of pixel-based manipulation tasks. Experimental results on the simulated tasks show that Whale-ST outperforms existing world model learning methods in both value estimation accuracy and video generation fidelity. Moreover, we demonstrate that Whale-ST, based on the retracing-rollout technique, effectively captures model prediction error and enhances offline policy optimization using imagined experiences. As a further step, we introduce Whale-X, a **414M-parameter** world model trained on **970k** real-world demonstrations from Open X-Embodiment datasets [13]. Whale-X serves as a foundational embodied world model for evaluating real-world behaviors. With fine-tuning on a few demonstrations in completely unseen environments and robots, Whale-X demonstrates strong OOD generalizability across visual, motion, and task perspectives. Furthermore, by scaling up the pre-training dataset or model parameters, Whale-X shows impressive scalability during both the pre-training and fine-tuning phases.

The primary contributions of this work are outlined as follows:

- We introduce WHALE, a framework for learning generalizable world models, consisting of two key techniques: *behavior-conditioning* and *retracing-rollout*, to address two major challenges in the application of world models to decision-making: **generalization** and **uncertainty estimation**;
- By integrating these two techniques from WHALE, we propose Whale-ST, a scalable spatial-temporal transformer-based world model designed for more effective decision-making, and further present Whale-X, a 414M-parameter world model pre-trained on 970K robot demonstrations;
- We conduct extensive experiments to demonstrate the remarkable scalability and generalizability of Whale-ST and Whale-X across both simulated and real-world tasks, highlighting their efficacy in enhancing decision-making.

2 Related Works

World models have a long research history and recently started to attract significant attention. World models were initially introduced under the name "action models" in simple tasks as components of the decision-making systems [14, 15] and were also referred to as "environment models" [16], "dynamics models" [17, 18], or simply "models" [19] in literature. Since the advent of the neural network era, dynamics models have been more widely applied in deep reinforcement learning algorithms to boost learning efficiency, resulting in a series of model-based reinforcement algorithms [19, 20, 8, 21, 18], while they focused primarily on environment modeling in lower-dimensional proprioceptive state spaces. [3] was the first to propose a general framework for modern world models with high-dimensional visual observations, where a vision module encodes the observed image into a compact latent vector to extract visual information at the current time step and a memory sequence model integrates the historical codes to create a representation that can predict future states. This generic architecture of world models soon achieved a series of notable successes in complex decision-making tasks [22, 23, 24, 25, 26].

Despite these successes achieved in world model learning, out-of-distribution generalization remains a fundamental challenge for world models, which has yet to be adequately addressed. In contrast to conventional supervised learning settings with no or mild OOD assumption where the target distribution is similar to the training data distribution, world models answer "what-if" questions: "*What will happen in the environment if the agent makes any possible decisions?*", which must be highly out-of-distribution. A potential solution to this generalization issue is collecting a larger amount of data to train large world models. Recently, advanced methods have leveraged modern action-conditioned video prediction models [27, 28] to model the visual dynamics and pre-train from large-scale video experience data [11, 29, 30]. Various sophisticated model architectures have been adopted in these methods, including RNNs [31, 22, 32], diffusion models [33, 34], and transformers [35, 36, 11]. Nevertheless, the available training data for model learning are usually collected by expert or near-expert policies, leading to low data coverage in state-action spaces, which poses challenges to reasoning decision outcomes for suboptimal policies in the learned world models [7].

Another line of work investigates the impact of learning methods on the generalizability of world models. For standard maximum likelihood objectives of single-step transitions, the autoregressive rollout errors or value gaps are linked to in-distribution error and policy divergence and are quadratically amplified by the rollout horizon, a phenomenon known as *compounding errors* [19, 37, 38]. To overcome the limitations in the standard MLE learning, a series of improvements have been made, including training multi-step models to reduce rollout errors [39, 40], using control objectives to train transition models [41, 42], adversarially training models for counterfactual target policies [4], learning dynamics reward to improve model generalization [43], contrastively learning energy transitions function [44], and incorporating policy information into model inputs to enable test-time model adaptation to target policies [9]. Despite the successes in lower-dimensional proprioceptive observation tasks, scaling these methods to large amounts of high-dimensional visual data remains absent. Introducing advanced learning methods suitable for training large world models with large-scale data to improve model generalizability is of unprecedented importance.

In addition to generalization, another key topic in world models for control is *uncertainty estimation*. It has been shown that offline decision-making within world models learned from partial-coverage data is vulnerable to the exploitation of model prediction errors [8, 45], which requires quantifying the prediction uncertainty of world models and reminding the agent to keep pessimistic about the model uncertainty [8, 46, 47, 18]. These typical algorithms estimate the model uncertainty via the ensemble of multiple models learned in parallel [48], which is quite computation-consuming, especially for large-scale tasks and models. Recent works [49, 50] adopt the entropy of the categorical token prediction distribution as an uncertainty indicator for large language models (LLMs), though there is limited support for its efficacy in offline model-based control.

3 Foundations of World Model Learning

3.1 Problem Formulation

A typical formulation of sequential decision tasks is the Markov decision process (MDP) [51, 52] specified by the tuple $\mathcal{M} = (\mathcal{S}, \mathcal{A}, r, T^*, \gamma, H, \rho_0)$, where \mathcal{S} is the state space, \mathcal{A} is the action space, $r(s, a)$ is the reward function, $T^*(s'|s, a)$ is the real transition probability, $\gamma \in (0, 1]$ is the discount factor, H is the decision horizon, and $\rho_0(s)$ is the initial state distribution. In this work, we simply consider the case where $\gamma = 1$ and $H < \infty$.

In reinforcement learning [53], the objective is to learn a policy that maximizes the expected return in the MDP, which involves estimating the value of different policies. Specifically, the value of policy π is defined as:

$$V_{T^*}^\pi = \mathbb{E}_{\tau_H \sim (\pi, T^*)} \left[\sum_{t=1}^H r(s_t, a_t) \right], \quad (1)$$

where the state-action trajectory $\tau_H = (s_1, a_1, \dots, s_H, a_H)$ and rewards are generated by the rollouts of policy π within the dynamics T^* . A common scenario involves abundant pre-collected experience data, but direct interaction with the environment is either prohibited or costly, necessitating value estimation to be performed offline.

An environment model T can be explicitly learned from the offline data to imitate the real state transition T^* , synthesizing imaginary experiences to simulate real environment interactions. For visual observation tasks, the agent cannot directly observe the states; instead, it receives high-dimensional images within the observation space \mathcal{O} , which normally introduces redundant information and partial observability. The visual world models [3] usually learn a vision module $E_\theta : \mathcal{O} \rightarrow \mathcal{S}$ to extract a compressed representation $z_t = E_\theta(o_t)$ from the current frame observation o_t , and use a sequence model to integrate the latent representations $z_{1:t}$ from past frames as well as actions $a_{1:t}$ to overcome the partial observability for future prediction. This architecture of world models empowers autoregressive imagination for any given policy, which enables policy evaluation and improvement without real-world interactions.

Assume that V_T^π is the value estimated within the model T , the environment model error induces a value gap $|V_{T^*}^\pi - V_T^\pi|$ for the policy π . If the model is globally accurate, the value gap will diminish for any policy. However, offline experiences are often collected by a narrow range of policies (e.g., near-expert policies). Therefore, the learned environment models are likely unfamiliar with the outcomes of novel decision patterns and are expected to generalize beyond the training experiences for counterfactual reasoning to evaluate diverse policies.

3.2 Generalizability of World Models

The common learning methods for world models regard the transition learning as a standard supervised learning problem, minimizing the negative log-likelihood (NLL) of the single-step transition probabilities over the pre-collected trajectories in a teacher-forcing manner, i.e.,

$$\min_T \mathbb{E}_{\mu \sim \Pi} \mathbb{E}_{\tau_H \sim (\mu, T^*)} \frac{1}{H} \sum_{h=1}^H -\log T(o_h | \tau_{h-1}) \iff \min_T l_{\text{KL}}(T; \Pi),$$

where (sub-)trajectory $\tau_h = (o_1, a_1, o_2, \dots, o_h, a_h)$, $1 \leq h \leq H$ is generated by interaction of a behavior policy μ with the real dynamics T^* , and behavior μ is assumed to be sampled from a behavior policy distribution Π . Minimizing the

NLL equals minimizing the KL divergence loss $l_{\text{KL}}(T; \Pi) = \mathbb{E}_{\mu \sim \Pi} \mathbb{E}_{\tau_H \sim (\mu, T^*)} \frac{1}{H} \sum_{h=1}^H D_{\text{KL}}(T^*(\cdot | \tau_{h-1}), T(\cdot | \tau_{h-1}))$.

The learned world models are usually utilized to evaluate any target policy π by simulating trajectories in an autoregressive manner:

$$V_T^\pi = \mathbb{E}_{\tau_H \sim (\pi, T)} \left[\sum_{t=1}^H r(o_t, a_t) \right],$$

where the trajectory simulation distribution deviates from the training distribution.

In classical sequential modeling tasks like sentence generation and translation, the distribution shift from teacher-forcing training to autoregressive generation diminishes as the model accuracy improves, which therefore does not lead to significant negative impacts. For world model learning, however, the distribution shift results from both the model prediction inaccuracy and the divergence between the target policy and behavior policies, exacerbating the evaluation inaccuracy:

$$\left| V_T^\pi - V_{T^*}^\pi \right| \leq 2R_{\max} \underbrace{H^2}_{\text{teacher-forcing}} \left(\underbrace{\sqrt{2 l_{\text{KL}}(T; \Pi)}}_{\text{in distribution error}} + \underbrace{L \cdot W_1(d^\pi, d^\Pi)}_{\text{policy divergence}} \right), \quad (2)$$

where a distribution shift term induced by the policy divergence³ occurs in addition to the KL training loss, further amplified by an H^2 factor caused by the supervised teacher-forcing learning. Even if the world model perfectly models the training distribution, i.e. $l_{\text{KL}}(T; \Pi) = 0$, the variation of the target policies could also significantly shift the trajectory simulation distribution to those large error areas, resulting in degenerative generalizability.

The generalization issue of world model learning has been noticed as a severe challenge even when large expert training data is available [7]. Previously, solutions have been proposed.

- Replacing the teacher-forcing objective by the distribution matching solves the compounding error [37], which reduces the term H^2 to H .

³Here $W_1(d^\pi, d^\Pi)$ is the Wasserstein-1 distance between the π -induced trajectory distribution $d^\pi(\tau)$ and the behavior trajectory distribution $d^\Pi(\tau) = \mathbb{E}_{\mu \sim \Pi}[d^\mu(\tau)]$, and L is the Lipschitz constant of model loss w.r.t. the trajectory, adapted from [9].

- Energy-based model can help reduce the in distribution error [44], which waives the need of fitting ill-shaped transition functions by neural networks.
- The adversarial counterfactual learning [4] alleviate the policy divergence issue.
- Learning an environment reward to constrain the world model can surprisingly help generalizes out of the data distribution [43].

Meanwhile, the above methods are all based on adversarial learning, which is hard to scaling up currently. In [9], a new way to enhance the generalizability was found, which learns to generalize during training by enforcing a policy condition. This paper inherits and improves this method.

4 Learning Generalizable World Models for Embodied Decision-making

Sequential decision-making within world models often necessitates agents to explore out-of-distribution (OOD) regions that go beyond the training dataset. This requires the world models to exhibit strong generalization capabilities, enabling it to make accurate predictions that closely mirror real-world dynamics. Meanwhile, reliably quantifying the prediction uncertainty, especially for transitions outside the world models’ effective generalization range, is essential for robust decision-making, which prevents offline policy optimization from exploiting erroneous model predictions. In consideration of these issues, we propose **WHALE**, a framework for learning generalizable world models with enhanced generalizability and efficient uncertainty estimation.

4.1 Behavior-conditioning for Generalization

According to the error decomposition in Eq (2), the generalization error of the world model primarily arises from error compounding caused by policy divergence. To reduce this error, one possible solution to this policy generalization issue is to embed the behavior information into the world model, allowing the model to actively recognize the behavior patterns of the policies and adapt to the policy-induced distribution shift [9]. This adaptation effect has been shown to reduce model generalization error caused by policy divergence, i.e. the last term in Eq (2). For further analysis, please refer to Appendix A. Building upon the concept of behavior-conditioning, we introduce a learning objective to obtain behavior embeddings from training trajectories and integrate the learned embeddings.

We would like to extract the decision patterns within training trajectories τ_H into a behavior embedding, reminiscent of the maximization of the evidence lower bound (ELBO) of the trajectory likelihood conditioned on the history τ_h [54, 55, 56]:

$$\log P(\tau_H|\tau_h) \geq \mathbb{E}_{q_\phi(z|\tau_H)} \sum_{t=h}^H \log \pi_w(a_t|o_t, \tau_{t-1}, z) - D_{\text{KL}}(q_\phi(z|\tau_H)||p_\psi(z|\tau_h)) + \text{Const}, \quad (3)$$

where $q_\phi(z|\tau_H)$ denotes the posterior encoder, encoding the whole trajectory τ_H into a latent variable z ; $\pi_w(a_h|o_h, \tau_{h-1}, z)$ denotes the decoder, which recovers the decision action from the latent variable z and the up-to-date history (τ_{h-1}, o_h) ; $p_\psi(z|\tau_h)$ denotes the prior predictor, which allows the prediction of z based on the history τ_h . The information bottleneck requires the learned variable z to effectively capture the decision pattern within the trajectory, embedding the information about the corresponding behavior policy. Following this argument, we propose to learn the behavior embedding by maximizing the ELBOs over H decision steps and adjusting the amount of KL constraints similar to β -VAE [57]:

$$\mathcal{L}(w, \phi, \psi) = \mathbb{E}_{\tau_H \sim \mathcal{D}} \left[\mathbb{E}_{q_\phi(z|\tau_H)} \left[- \sum_{h=1}^H \log \pi_w(a_h|o_h, \tau_{h-1}, z) \right] + \beta \sum_{h=1}^H D_{\text{KL}}(q_\phi(z|\tau_H)||p_\psi(z|\tau_h)) \right], \quad (4)$$

here the KL terms constrain the embedding predictions from sub-trajectories up to each time step h , encouraging them to approximate the posterior encoding. This ensures that the representation remains policy-consistent, meaning that trajectories generated by the same policy exhibit similar behavioral patterns and, consequently, similar representations.

The learned prior predictor p_ψ is then used to obtain behavior embeddings z_h from history τ_h for behavior-conditioning during world model learning, where the behavior embeddings are accepted as additional covariates for future prediction:

$$\min_T \mathbb{E}_{\mu \sim \Pi} \mathbb{E}_{\tau_H \sim (\mu, T^*)} \frac{1}{H} \sum_{h=1}^H \mathbb{E}_{z_h \sim p_\psi(\cdot|\tau_h)} - \log T(o_{h+1}|\tau_h, z_h).$$

When rolling out target policies or executing action sequences within the learned world models, the prior predictor infers the latent behavior intentions from interaction history, enabling the autoregressive generation process to adjust to the target distribution on the fly for future imagination adaptively.

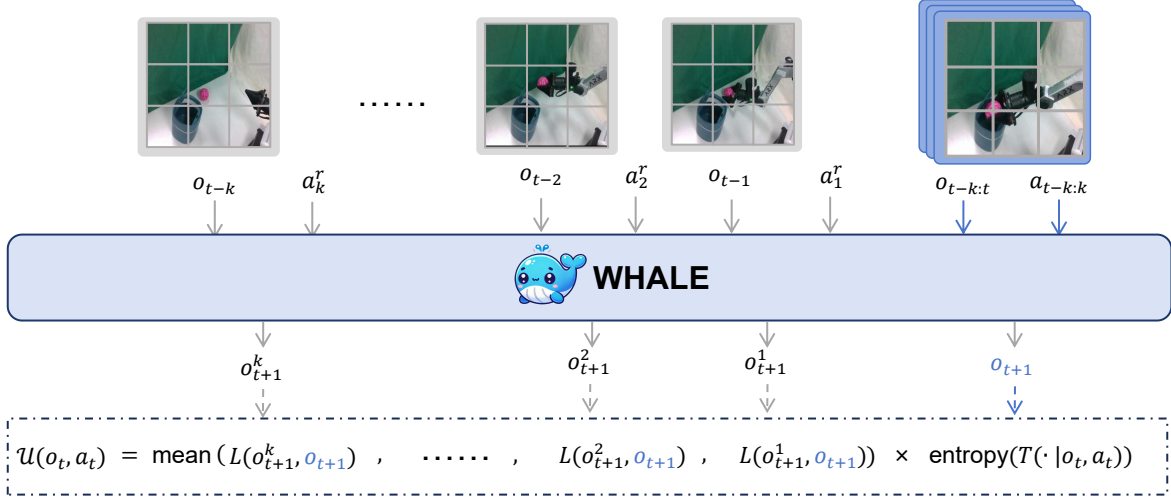


Figure 2: Illustration of retracing-rollout uncertainty quantifier.

4.2 Retracing-rollout for Uncertainty Estimation

Agents can take any actions in world models to generate an imagined future, which may significantly diverge from the offline dataset. As a result, world models inevitably produce inaccurate and unreliable samples. Previous works have demonstrated, both theoretically and experimentally, that if we use model-generated data without restrictions, the performance of the policy can be severely undermined [8, 45]. Therefore, uncertainty estimation is essential for world models, as it can indicate when to trust our models.

Previous ensemble-based uncertainty estimation methods for world models often require training multiple models [48, 18], making them computationally expensive, especially for large-scale tasks and complex models. Beyond these, any-step uncertainty estimation [58] has emerged as a computationally efficient alternative, leveraging discrepancies in predictions across historical information of varying lengths, without relying on ensemble. However, any-step is specifically designed for recurrent neural networks and cannot be directly applied to transformers, limiting its scalability and applicability in real-world tasks. To overcome this limitation, we introduce a novel uncertainty estimation method, **retracing-rollout**, inspired by the concept of variable-length history in any-step. The core innovation of retracing-rollout lies in the introduction of **retracing-action**, which leverages the semantic structure of the action space in embodied control, enabling more accurate and efficient uncertainty estimation for transformer-based world models.

We begin by introducing retracing-action. Concretely, retracing-action serves as an equivalent substitute for any given action sequence. For an action sequence $a_{1:k}$, its corresponding retracing-action is defined as a_k^r , with the goal that the outcome o_{k+1} produced by the robotics executing action sequence $a_{1:k}$ from any observation o_1 nearly identical to the outcome o_{k+1}^r produced when executing the retracing-action a_k^r . Benefiting from the semantic structure of the action space in embodied control, the retracing-action is computationally feasible for end-effector pose control. For instance, in the Open X-embodied dataset, the action space is defined by a 7-dimensional vector that controls the end-effector. The first three dimensions represent the changes in the gripper position ($\Delta x, \Delta y, \Delta z$), the next three represent the changes in wrist orientation ($\Delta \text{roll}, \Delta \text{pitch}, \Delta \text{yaw}$), and the final dimension determines whether the gripper opens or closes. Therefore, the retracing-action can be directly computed using Eq (5), where $a_i^{(j)}$ represents the value of the j -th dimension of the action a_i .

$$a_k^r = \left(\sum_{i=1}^k a_i^{(0)}, \dots, \sum_{i=1}^k a_i^{(5)}, a_k^{(6)} \right). \quad (5)$$

The next concept is retracing-rollout. Given a retracing step k , the process begins by backtracking to o_{t-k} as the starting frame for a rollout. The corresponding retracing-action a_k^r for action sequence $a_{t-k:k}$ is executed from o_{t-k} , yielding the corresponding outcome o_{k+1} . In practice, to prevent multi-step cumulative retracing-action a_k^r from exceeding the action-space range, a_k^r is divided into k steps. In each step, the first six dimensions are set to $\frac{1}{k} a_k^{r(i)}$, while the last dimension, $a_k^{r(6)}$, remains constant, allowing us to achieve desired outcomes through a multi-step rollout.

Finally, we present the retracing-rollout uncertainty quantifier, as illustrated in Figure 2. To estimate uncertainty for (o_t, a_t) , various retracing steps are set to generate corresponding retracing-rollout predictions. We then calculate

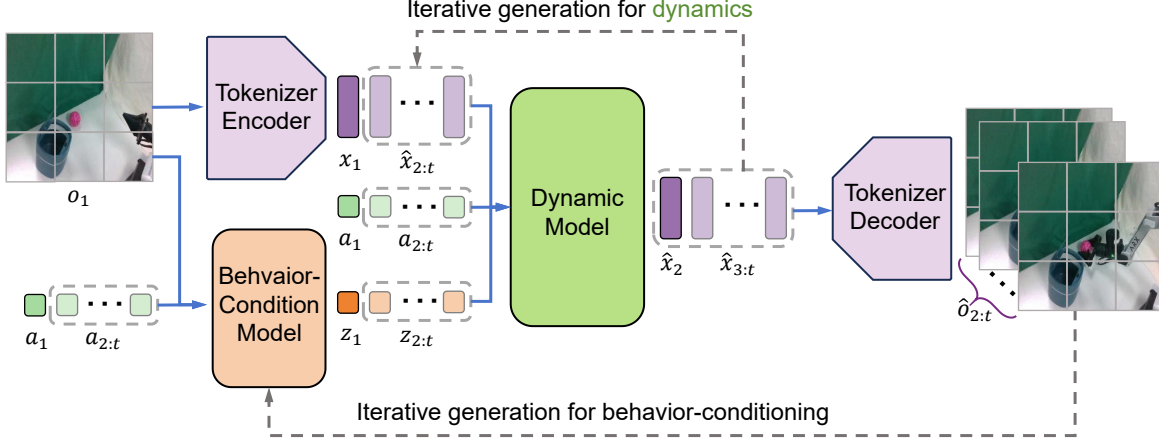


Figure 3: Overall architecture of Whale-ST. The behavior-conditioning model encodes the observation and action subsequences into behavior embedding z_i , which are then passed to the dynamics model along with observation tokens and actions to generate the next token predictions \hat{x}_{i+1} . The predicted observation tokens are subsequently fed into the dynamics model for further predictions autoregressively and decoded into observation predictions to obtain later behavior embeddings.

the feature-level disagreement, represented as perceptual loss, between outputs generated from retracing-rollout and the output without retracing-rollout. Additionally, we incorporate the predictive entropy of the dynamics model $\text{entropy}(T(\cdot|o_t, a_t))$, which is typically used to measure the confidence of the model itself. By multiplying the average disagreement and predictive entropy, we derive the final uncertainty estimation result. Notably, retracing-rollout does not require any modifications during the training phase, which significantly reduces the computational overhead compared to ensemble-based methods.

5 Practical Implementation of WHALE

In this section, we present an instantiation of WHALE, Whale-ST, a scalable world model with ST-transformer architecture. As a further step, we introduce Whale-X, a 414M-parameter world model trained on 970k real-world demonstrations from Open X-Embodiment datasets.

5.1 Instantiation with ST-transformer architecture: Whale-ST

Figure 3 illustrates the overall architecture of Whale-ST. Specifically, Whale-ST comprises three main components: behavior-conditioning model, video tokenizer, and dynamics model. Inspired by previous works [11], these modules utilize a spatial-temporal transformer (ST-transformer) architecture. Within this framework, each token is designed to attend only to other tokens in the current frame and those at corresponding positions in prior frames. Additionally, Whale-ST can generate all tokens for the next frame in parallel at one time. These designs significantly simplify the computational demands from a quadratic to a linear dependency relative to sequence length, reducing both the memory usage and computational costs of the model training while increasing model inference speed.

5.1.1 Behavior-conditioning Model Learning

Behavior-conditioning model comprises a CNN-based visual encoder v_θ , ST-Transformer-based posterior model q_ϕ , prior model p_ψ , and reconstruction model π_ω . Given an input image sequence, v_θ first converts it into tokens by patchifying the images. These tokens are then processed by q_ϕ , p_ψ , and π_ω , which produce the posterior representations z_H , prior representations z_h , and reconstructed actions a_h , respectively. As a results, we can train the behavior-conditioning model using the loss function defined in Eq (4). For behavior embeddings, we employ two-hot encoding due to its strong expressive capacity and stable training process, as noted in [22].

5.1.2 World Model Learning

World models typically consist of an observation encoder that encodes the raw observation into a compact representation and a dynamics model that predicts future transitions within this representation space [3]. In this work, we adopt a

tokenizer based on VQ-VAE [59] as the encoder to discretize observations into tokens and train a dynamics model at the token level.

Specifically, the video tokenizer e_θ is composed of an encoder E_θ and a decoder D_θ , where the encoder E_θ compresses video input into a sequence of tokens, while the decoder D_θ is capable of reconstructing the original video from these tokens. This tokenizer is trained with the standard VQ-VAE loss $\mathcal{L}_{\text{tok}}(\theta)$, which is a combination of a L_1 reconstruction loss, a codebook loss, and a commitment loss.

After training the tokenizer, we embed the policy information into the dynamics model learning process. The key distinction from standard dynamics model learning is that Whale-ST additionally incorporates a behavior-conditioning z_h inferred by the prior predictor p_ψ . In this phase, for each input trajectory segment τ_H , the video tokenizer first converts it into a sequence of tokens $x_H = ((x_1^{(1)}, \dots, x_1^{(N)}), (x_2^{(1)}, \dots, x_2^{(N)}), \dots, (x_H^{(1)}, \dots, x_H^{(N)}))$, where $x_i^{(j)}$ represents the j -th token of the i -th frame. Consequently, the training objective of the dynamics model is to maximize the log-likelihood of the tokens x_{h+1} for the next frame s_{h+1} , conditioned on the history tokens $x_{0:h}$, history actions $a_{0:h}$ and the behavior-conditioning $z_h = p_\psi(\tau_h)$:

$$\mathcal{L}_{\text{dyn}}(\theta) = \mathbb{E}_{\tau_H \sim \mathcal{D}} \left[- \sum_{h=1}^H \log P_\theta(x_{h+1} | x_{1:h}, a_{1:h}, z_h) \right], \quad (6)$$

Intuitively speaking, Whale-ST not only accepts history as a direct feature to predict transitions but also infers the latent decision intention from the history to enable test-time adaptation to the induced distribution shift.

5.2 Pre-training on real-world robot demonstrations: Whale-X

We introduce Whale-X, a 414M-parameter world model pre-trained on 970K real-world robot demonstrations from the Open X-Embodiment dataset. The entire dataset is utilized to pre-train both the behavior-conditioning model and the video tokenizer, while a focused subset of the data is used to pre-train the dynamics model. Whale-X serves as a foundational embodied world model for assessing real-world behaviors, capable of generating realistic, controllable video trajectories that align closely with specified actions, as illustrated in Figure 1.

Data. Whale-X is pre-trained on the Open X-Embodiment dataset [13] (OpenX), a comprehensive dataset consists of more than 70 individual robot datasets, with more than 2M robot trajectories pooled into a coherent and easy-to-use data format in a large community effort. Follow [60], our pre-training dataset collection includes 27 datasets, with a total scale of 970k demonstrations, we list our used data mixture and weights in Table 11. To train a world model focused on tabletop tasks, we extract data related to tabletop tasks from the dataset that features similar camera positions (the bolded tasks in Table 11) to train the dynamics model, while the video tokenizer and behavior-conditioning model are trained on the full OpenX dataset.

6 Experiment

We conduct extensive experiments on both simulated tasks and real-world tasks. The experimental design is primarily designed to answer the following key questions:

- How does Whale-ST perform compared with other baselines on simulated tasks? Are behavior-conditioning and retracing-rollout techniques effective? (Section 6.1)
- How does Whale-X perform on real-world tasks? Can Whale-X benefit from pre-training on internet-scale data? (Section 6.2)
- How is the scalability of Whale-X? Does increasing the model capacity or pre-training data improve performance on real-world tasks? (Section 6.3)

6.1 Whale-ST on Simulated Tasks

6.1.1 Experiment Setups

We conduct our simulated task experiments on the Meta-World [12] benchmark, which offers a diverse set of vision-based manipulation tasks. In this experiment, we construct a training dataset with 60k trajectories collected from 20 tasks. The model learning algorithms are required to use all the data for training from scratch. Afterward, we conduct model evaluation and uncertainty estimation experiments to validate the effectiveness of behavior-conditioning and retracing-rollout, respectively. More detailed information about data collection can be found in Appendix C.1.

6.1.2 Model Evaluation

Baselines. We compare Whale-ST against several world model learning baselines, including (1) **FitVid** [32], a variational-based world model that can fit large diverse video datasets. (2) **MCVD** [33], a diffusion-based world model that can perform video generation conditioning on different subsets of video frames and actions. (3) **DreamerV3** [24], a recurrent world model that outperforms specialized methods across diverse control tasks. (4) **iVideoGPT** [36], a scalable transformer-based world model that achieved state-of-the-art results in video generation and embodied control tasks. Complete descriptions and implementation details are provided in Appendix B.3.

Evaluation Metrics. We assess the performance of world models from two perspectives: (1) **Value estimation accuracy.** Verifies whether the model can correctly estimate the value of a given action sequence, in terms of Value Gap, Return Correlation, and Regret [5]. (2) **Video fidelity.** Measures the quality of video trajectory generation, in terms of FVD [61], PSNR [62], LPIPS [63], and SSIM [64]. More detailed information about evaluation metrics is provided in Appendix B.4.

Task Results. Table 1 presents the results for value prediction accuracy, where Whale-ST demonstrates exceptional performance across all three metrics. At a 64×64 resolution, Whale-ST achieves a value gap closely aligning with DreamerV3’s top score. Moreover, it surpasses all other models on return correlation and regret@5, highlighting minimal prediction errors. When tested at a higher resolution of 256×256 , the performance of Whale-ST further improves, achieving the smallest value gap and the highest return correlation, reflecting an even finer understanding of environment dynamics. With the lowest regret, Whale-ST provides high-confidence guidance for decision-making. Furthermore, Table 2 presents the results for video fidelity, showing that Whale-ST consistently outperforms all other methods across metrics related to video fidelity, with a notable advantage in FVD.

Ablation Study. To validate the effectiveness of behavior-conditioning, we conduct ablation experiments at a resolution of 256×256 , as shown in the last two rows of Table 1 and 2. Incorporating behavior-conditioning markedly improves value prediction accuracy in world models, reducing the value gap by 18% and regret by 22%. Furthermore, behavior-conditioning consistently enhances video fidelity across all metrics.

Meta-World	#Params	Value Gap↓	Return Correlation↑	Regret@5↓
<i>64×64 resolution</i>				
FitVid	143M	18.2	0.64	22.0
MCVD	53M	20.6	0.72	12.2
DreamerV3	44M	10.0	0.70	16.5
iVideoGPT	63M	15.9	0.62	7.2
Whale-ST (ours)	51M	10.3 ± 0.8	0.77±0.01	7.3±1.2
<i>256×256 resolution</i>				
DreamerV3	61M	11.7	0.72	11.5
Whale-ST (w/o bc)	63M	11.8±0.4	0.84±0.01	5.0±0.3
Whale-ST (ours)	63M	9.7±0.1	0.86±0.01	3.9±0.3

Table 1: Value prediction accuracy comparison on Meta-World benchmark with various models.

Meta-World	#Params	FVD↓	PSNR↑	SSIM↑	LPIPS↓
<i>64×64 resolution</i>					
FitVid	143M	154.6	23.7	90.3	6.5
MCVD	53M	272.8	29.7	92.3	4.0
DreamerV3	44M	142.7	27.6	92.1	4.3
iVideoGPT	63M	115.7	28.5	92.8	4.5
Whale-ST (ours)	51M	38.5±2.6	28.8±0.0	93.5±0.1	3.7±0.1
<i>256×256 resolution</i>					
DreamerV3	61M	112.4	26.2	91.7	8.5
Whale-ST (w/o bc)	63M	32.0±0.4	28.9±0.2	94.6±0.1	4.6±0.1
Whale-ST (ours)	63M	28.2±3.6	29.2±0.2	95.0±0.1	4.3±0.1

Table 2: Video fidelity comparison on Meta-World benchmark with various models.

6.1.3 Uncertainty Estimation

Baselines. We compare the retracing-rollout technique with two baseline methods for uncertainty estimation: (1) **Entropy-based Method:** We use the predictive entropy of the transformer-based dynamics model to quantify uncertainty, following approaches similar to those in [49, 50]. (2) **Ensemble-based Method:** We independently train three dynamics models and estimate uncertainty by measuring the pixel-level disagreement between images generated by each model, following methods described in [65]. Detailed baseline implementations are provided in Appendix B.3.

Evaluation Metrics. We evaluate uncertainty estimation methods from two perspectives: (1) **Model Error Prediction.** We evaluate uncertainty by treating uncertainty estimation as the problem of predicting whether to trust the generated trajectory with given observations and actions. Therefore, we compute the correlation between the estimated uncertainty and the perceptual model error, defined as the perceptual loss between real observations and generated samples. A higher correlation suggests a more reliable uncertainty estimation. (2) **Offline Reinforcement Learning.** According to [8], offline model-based reinforcement learning (offline MBRL) relies on estimating the fidelity of generated samples to support conservative policy learning, where more accurate uncertainty estimates lead to improved and more stable policies. Consequently, we also evaluate how effectively the estimated uncertainty contributes to model-based policy optimization in offline MBRL. Following previous works [8, 16], we use the estimated uncertainty to reshape the reward, i.e., $r'(s, a) = r(s, a) - \alpha \mathcal{U}(s, a)$, where $r(s, a)$ is the original reward and α is a hyperparameter determines the extent of the uncertainty penalty. Appendix B.4 provides more detailed information about evaluation metrics.

Task Results. Table 3 demonstrates the model error prediction results, showing that retracing rollout consistently outperforms other baselines in all 5 tasks. Specifically, compared to the ensemble-based method, retracing rollout achieves a significant 500% improvement, and compared to the entropy-based method, it shows a 50% increase. Additional results are available in Appendix E.2. Furthermore, Figure 4 displays the offline MBRL outcomes, where retracing rollout achieves superior convergence performance and training stability in three of the five tasks while performing comparably in the remaining two. Notably, in *faucet-close* and *plate-slide* tasks, retracing rollout is the only method capable of stable convergence, whereas other methods experience varying degrees of performance decline in later training stages. Additionally, compared to learning without an uncertainty penalty, all methods deliver significant improvements, further confirming the importance of uncertainty estimation in policy learning.

Tasks	Ensemble-based	Entropy-based	Retracing Rollout (ours)
plate-slide	0.14±0.01	0.31±0.08	0.55±0.09
button-press-wall	0.11±0.01	0.31±0.03	0.52±0.07
faucet-close	0.06±0.05	0.40±0.03	0.70±0.01
coffee-push	0.06±0.01	0.49±0.06	0.53±0.04
handle-press	0.10±0.07	0.25±0.06	0.45±0.08
Average	0.10±0.03	0.35±0.05	0.55±0.06

Table 3: Correlation between estimated uncertainty and perceptual model error.

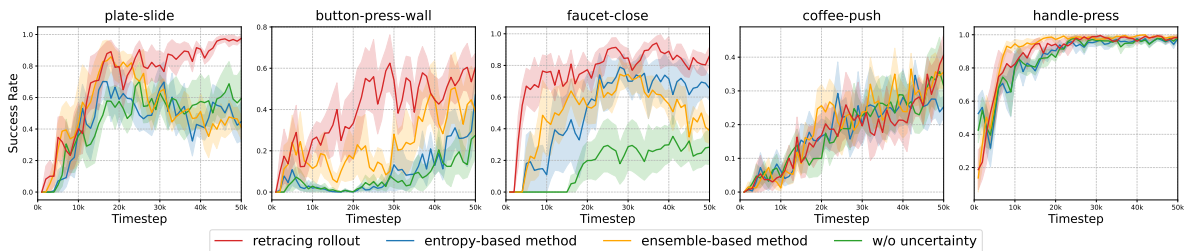


Figure 4: Offline reinforcement learning with different uncertainty estimation methods.

6.2 Whale-X on Real-world Tasks

6.2.1 Experiment Setups

To evaluate the generalizability of Whale-X in the physical world, we conduct comprehensive real-world experiments on ARX5 robotic platform. The evaluation tasks differ significantly from the pre-training data, in terms of the robotic platform, camera angles, and background visual information, posing considerable challenges for world models.

We carefully collect a limited dataset for fine-tuning, consisting of 60 trajectories for each of the four tasks: *open bin*, *push plate*, *throw ball*, and *move bottle*. Following this, we designed several challenging unseen tasks for testing, with a focus on evaluating the model from the perspectives of *visual generalization*, *motion generalization*, and *task generalization* perspectives. Further details on the fine-tuning and data collection process can be found in Appendix B.2 and Appendix D respectively.

6.2.2 Model Evaluation

Evaluation Metrics. For a visual world model to be effective in decision-making, the world model needs to focus more on reasoning about the consequences of actions than on reconstructing irrelevant visual information like backgrounds. Thus we introduce the *consistency rate* to assess whether the differences in reconstructed object positions, interactive object states, and robot arm positions fall within an acceptable range compared to the ground truth. We use the multimodal large model GPT-4o [66] for this evaluation through multiple rounds of Q&A. Details of the prompts and the evaluation process can be found in Appendix F, with results presented in Figure 5. In addition, we employ several video fidelity metrics, similar to those in Section 6.1, to assess the quality of video generation by the world models.

Task Results

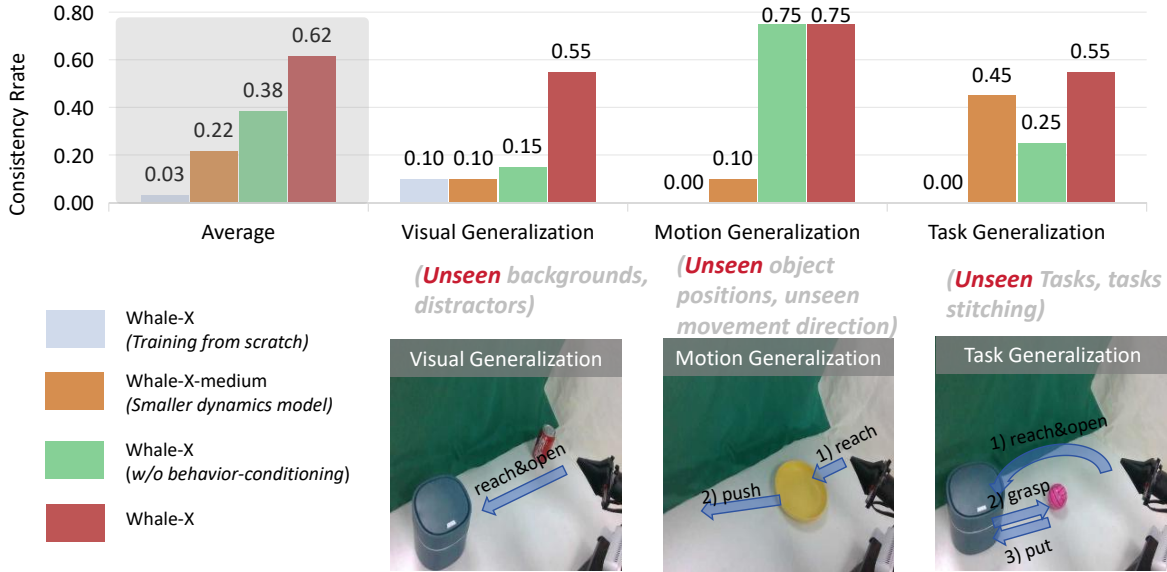


Figure 5: Physical robot evaluation on unseen scenarios. The row above shows the bar chart of the consistency rate, and the row below represents the tasks used for testing. The experiments demonstrate that Whale-X exhibits good generalization performance in unseen scenarios.

Real-world Tasks	PSNR↑	SSIM↑	LPIPS↓
<i>unseen tasks & 256×256 resolution</i>			
Whale-X-base (training from scratch)	20.0	74.9	37.0
Whale-X-base (w/o behavior-conditioning)	21.4	79.0	31.2
Whale-X-medium (77M parameter)	21.9	79.9	30.0
Whale-X (ours)	22.3	80.5	29.6

Table 4: Video fidelity of Whale-X on real-world tasks.

Whale-X shows a clear advantage in our real-world experiments. Specifically, as shown in Figure 5, the quantitative results indicate that: 1) Whale-X improves consistency by **63%** compared to models without behavior-conditioning, demonstrating that these mechanisms significantly enhance the OOD generalizability; and 2) Whale-X, pre-trained on 970k samples, achieved much higher consistency rate than models trained from scratch, highlighting the benefits of pre-training on large-scale internet data. 3) Increasing the model parameters improves the generalizability of the world model. Whale-X-base with 203M parameters dynamics model achieves a consistency rate that is about three times higher than the 77M version across three unseen tasks. Furthermore, the evaluation of video generation quality aligns with these consistency rate findings as illustrated in Table 4. The behavior-conditioning technique, pre-trained on

large-scale datasets, combined with scaling up model parameters, significantly enhances OOD generalizability from a video fidelity perspective.

6.2.3 Uncertainty Estimation

Evaluation Metrics. In contrast to simulated tasks, obtaining a pixel-based reward function in real-world tasks is nearly impossible, which makes it challenging to optimize policies directly through reinforcement learning within the world model. To overcome this limitation, we calculate cumulative uncertainty for each generated trajectory using retracing rollout and then select the top $k\%$ of trajectories with the lowest cumulative uncertainty. For these selected trajectories, we compute the consistency rate as an evaluation metric. Intuitively, if uncertainty accurately measures model error, lower uncertainty should correspond to more realistic generated trajectories, which are expected to yield a higher consistency rate.

Task Results. Figure 6 presents the results of uncertainty estimation in real-world tasks, illustrating how the filtered proportion of trajectories affects the consistency rate. The gray line represents the average consistency rate across three tasks. The results show that reducing the number of selected trajectories—thus lowering the uncertainty threshold—leads to a marked increase in consistency rate. Notably, when $k = 5$, the filtered trajectories align with real outcomes with 100% accuracy. We observe a slight decrease in the consistency rate for visual generalization tasks at $k = 10, 25$, and 50. In these cases, the estimated uncertainty tends to reflect model error on unseen backgrounds more than task-specific information, which could be one of the improvements for future work.

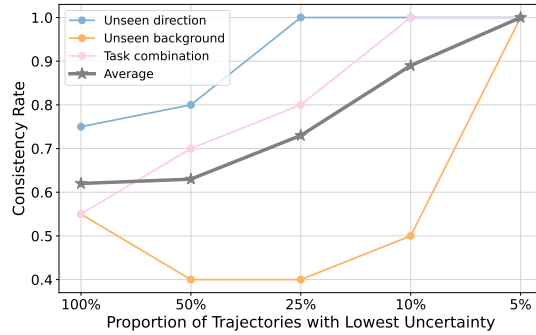


Figure 6: Consistency rate with different proportions of trajectories with the lowest uncertainty.

6.3 Scaling Experiments

In this section, we aim to investigate the scaling behavior of Whale-X. Specifically, We freeze the video tokenizer and behavior-conditioning model, adjusting only the model size and pre-training data size of dynamics models, considering the impact of model size and data size for the pre-training and fine-tuning phases.

Pre-training Scaling Experiments. With a frozen video tokenizer and behavior-conditioning model, we train four dynamics models ranging from 39M to 456M parameters during the pre-training phase, with results shown in the first two plots of Figure 7. These results demonstrate that Whale-X exhibits strong scalability, as increasing either the pre-training data or the number of parameters reduces the training loss. Notably, the training loss of Whale-X follows a log-linear relationship with FLOPs, which can guide the design of larger models and appropriate data ratios for future experiments.

Fine-tuning Scaling Experiments. Apart from the scalability in the pre-training stage, it is also worth verifying whether a larger model can exhibit better performance during the fine-tuning phase. To this end, we fine-tune a series of dynamics models and show the test mean-squared-error losses in the leftmost plot in Figure 7. The results indicate that after fine-tuning, the larger model demonstrates lower loss on test data, highlighting the promising scalability of Whale-X for real-world tasks.

6.4 Visualization Results

Qualitative Evaluation. Figure 1 demonstrates the qualitative evaluation results on Meta-World, Open X-Embodiment, and our real-world tasks. The results show that Whale-ST and Whale-X can generate high-fidelity video trajectories for long-horizon rollouts, maintaining visual quality and consistency over extended sequences. More qualitative evaluation results are provided in Appendix E.1.

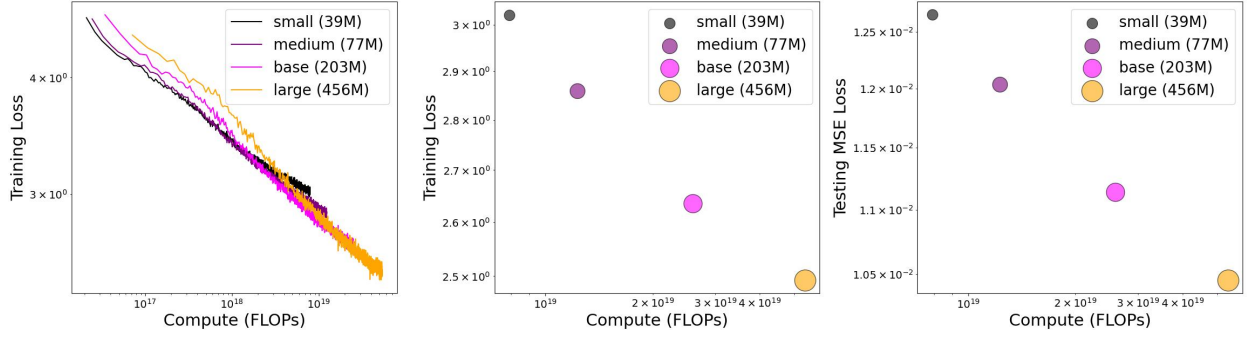


Figure 7: Scaling experiment results of Whale-X. The leftmost plot shows the training loss curves for models with varying parameter sizes during the pre-training phase. The second plot presents the final training loss for all models after 300k pre-training steps. The third plot displays the test loss after fine-tuning. The legend in the figure indicates the parameter number of the dynamics model.

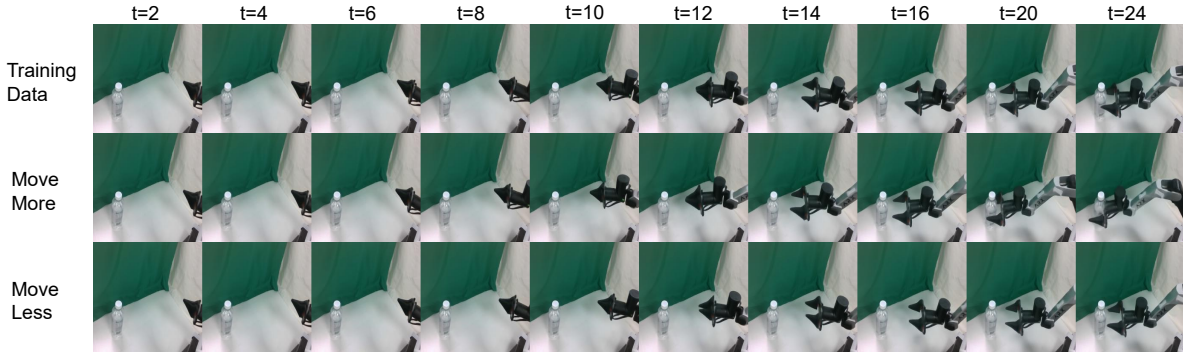


Figure 8: Controllable generation of Whale-X. Given an action sequence $a_{0:t}$, the first row shows the generated trajectory by interactively executing $a_{0:t}$ in Whale-X. The second row presents the "move more" trajectory generated by executing $1.2 \cdot a_{0:t}$, and the third row shows the "move less" trajectory generated by executing $0.8 \cdot a_{0:t}$.

Controllable Generation. Figure 8 demonstrates the strong controllability and generalizability of Whale-X. Given an unseen action sequence, Whale-X can generate videos that align with human understanding, learning the causality between actions and robotic arm displacement.

Behavior-conditioning Visualization. To verify whether the learned behavior embedding has captured policy modes, we perform t-SNE [67] to visualize the representations corresponding to different tasks and policies. Figure 15a shows that different policies for the same task can be distinguished by the learned behavior embedding. Notably, the embedding of the noisy expert policy appears to be a linear interpolation between the expert policy and the noisy policy, indicating that the behavior-conditioning models the policies reasonably. Figure 15b shows that the expert policies for different tasks can also be distinguished, while Figure 15c shows the random policies for different tasks cannot. This distinction indicates that our learned embedding is more inclined toward policy representation rather than task representation.

7 Discussions and Limitations

In this paper, We introduce WHALE, a framework of world model learning that incorporates the behavior-conditioning mechanism and retracing-rollout technique to enhance out-of-distribution generalization and efficient uncertainty estimation. Building on this foundation, we present Whale-ST, a scalable ST-transformer-based world model, and pre-train a 414M-parameter Whale-X on large-scale real-world robot data to assist physical robot manipulation. As a powerful world model with strong generalizability and promising scalability, Whale-X enables high-fidelity imagination and accurate value estimation, even in novel scenarios, thereby facilitating downstream control tasks.

Limitations and future work. Although WHALE marks significant progress, there remains substantial room for further improvement in future work. One limitation is the lack of diversity in real-world robotic data, typically collected by a narrow range of policies (e.g. near-optimal policies). This poses significant challenges to the generalization

of world models. Additionally, we found that the quality of reward models with visual input plays a crucial role in accurate value estimation, which remains an unsolved challenge for future research. Lastly, we have to mention that although the generalization capability of Whale-ST and Whale-X has significantly improved compared with previous methods, it remains limited for zero-shot transfer in the face of the diversity and complexity of unseen real-world tasks. Integrating existing prior knowledge into the data-driven world model learning process could enable broader generalization, presenting a valuable avenue for long-term research.

References

- [1] Gerrit W Maus, Jason Fischer, and David Whitney. Motion-dependent representation of space in area mt+. *Neuron*, 78(3):554–562, 2013.
- [2] Nora Nortmann, Sascha Rekauszke, Selim Onat, Peter König, and Dirk Jancke. Primary visual cortex represents the difference between past and present. *Cerebral Cortex*, 25(6):1427–1440, 2015.
- [3] David Ha and Jürgen Schmidhuber. World models. *CoRR*, abs/1803.10122, 2018.
- [4] Xiong-Hui Chen, Yang Yu, Zhengmao Zhu, Zhihua Yu, Chen Zhenjun, Chenghe Wang, Yinan Wu, Rong-Jun Qin, Hongqiu Wu, Ruijin Ding, et al. Adversarial counterfactual environment model learning. *Advances in Neural Information Processing Systems*, 36:70654–70706, 2023.
- [5] Justin Fu, Mohammad Norouzi, Ofir Nachum, George Tucker, Ziyu Wang, Alexander Novikov, Mengjiao Yang, Michael R. Zhang, Yutian Chen, Aviral Kumar, Cosmin Paduraru, Sergey Levine, and Tom Le Paine. Benchmarks for deep off-policy evaluation. In *9th International Conference on Learning Representations, ICLR 2021, Virtual Event, Austria, May 3-7, 2021*, 2021.
- [6] Sergey Levine, Aviral Kumar, George Tucker, and Justin Fu. Offline reinforcement learning: Tutorial, review, and perspectives on open problems. *arXiv preprint arXiv:2005.01643*, 2020.
- [7] Ingmar Schubert, Jingwei Zhang, Jake Bruce, Sarah Bechtle, Emilio Parisotto, Martin Riedmiller, Jost Tobias Springenberg, Arunkumar Byravan, Leonard Hasenclever, and Nicolas Heess. A generalist dynamics model for control. *arXiv preprint arXiv:2305.10912*, 2023.
- [8] Tianhe Yu, Garrett Thomas, Lantao Yu, Stefano Ermon, James Y. Zou, Sergey Levine, Chelsea Finn, and Tengyu Ma. MOPO: model-based offline policy optimization. In *Advances in Neural Information Processing Systems 33 (NeurIPS’20)*, virtual event, 2020.
- [9] Ruifeng Chen, Xiong-Hui Chen, Yihao Sun, Siyuan Xiao, Minhui Li, and Yang Yu. Policy-conditioned environment models are more generalizable. In *Forty-first International Conference on Machine Learning*, 2024.
- [10] Ju Ma, Juan Zhao, and Yao Hou. Spatial-temporal transformer networks for traffic flow forecasting using a pre-trained language model. *Sensors*, 24(17):5502, 2024.
- [11] Jake Bruce, Michael Dennis, Ashley Edwards, Jack Parker-Holder, Yuge Shi, Edward Hughes, Matthew Lai, Aditi Mavalankar, Richie Steigerwald, Chris Apps, et al. Genie: Generative interactive environments. *arXiv preprint arXiv:2402.15391*, 2024.
- [12] Tianhe Yu, Deirdre Quillen, Zhanpeng He, Ryan Julian, Karol Hausman, Chelsea Finn, and Sergey Levine. Meta-world: A benchmark and evaluation for multi-task and meta reinforcement learning. In *Conference on robot learning*, pages 1094–1100. PMLR, 2020.
- [13] Abby O’Neill, Abdul Rehman, Abhinav Gupta, Abhiram Maddukuri, Abhishek Gupta, Abhishek Padalkar, Abraham Lee, Acorn Pooley, Agrim Gupta, Ajay Mandlekar, et al. Open x-embodiment: Robotic learning datasets and rt-x models. *arXiv preprint arXiv:2310.08864*, 2023.
- [14] Richard S Sutton. Integrated architectures for learning, planning, and reacting based on approximating dynamic programming. In *Machine learning proceedings 1990*, pages 216–224. Elsevier, 1990.
- [15] Richard S Sutton. Dyna, an integrated architecture for learning, planning, and reacting. *ACM Sigart Bulletin*, 2(4):160–163, 1991.
- [16] Marc Rigter, Bruno Lacerda, and Nick Hawes. Rambo-rl: Robust adversarial model-based offline reinforcement learning. *Advances in neural information processing systems*, 35:16082–16097, 2022.
- [17] Yuping Luo, Huazhe Xu, Yuanzhi Li, Yuandong Tian, Trevor Darrell, and Tengyu Ma. Algorithmic framework for model-based deep reinforcement learning with theoretical guarantees. In *International Conference on Learning Representations*, 2019.

- [18] Yihao Sun, Jiaji Zhang, Chengxing Jia, Haoxin Lin, Junyin Ye, and Yang Yu. Model-bellman inconsistency for model-based offline reinforcement learning. In *Proceedings of the 40th International Conference on Machine Learning (ICML'23)*, Honolulu, HI, 2023.
- [19] Michael Janner, Justin Fu, Marvin Zhang, and Sergey Levine. When to trust your model: Model-based policy optimization. *Advances in neural information processing systems*, 32, 2019.
- [20] Kurtland Chua, Roberto Calandra, Rowan McAllister, and Sergey Levine. Deep reinforcement learning in a handful of trials using probabilistic dynamics models. *Advances in neural information processing systems*, 31, 2018.
- [21] Tianhe Yu, Aviral Kumar, Rafael Rafailov, Aravind Rajeswaran, Sergey Levine, and Chelsea Finn. COMBO: conservative offline model-based policy optimization. In *Advances in Neural Information Processing Systems 34 (NeurIPS'21)*, virtual event, 2021.
- [22] Danijar Hafner, Timothy Lillicrap, Jimmy Ba, and Mohammad Norouzi. Dream to control: Learning behaviors by latent imagination. In *International Conference on Learning Representations*, 2020.
- [23] Danijar Hafner, Timothy P Lillicrap, Mohammad Norouzi, and Jimmy Ba. Mastering atari with discrete world models. In *International Conference on Learning Representations*, 2021.
- [24] Danijar Hafner, Jurgis Pasukonis, Jimmy Ba, and Timothy Lillicrap. Mastering diverse domains through world models. *arXiv preprint arXiv:2301.04104*, 2023.
- [25] Nicklas A Hansen, Hao Su, and Xiaolong Wang. Temporal difference learning for model predictive control. In *International Conference on Machine Learning*, pages 8387–8406. PMLR, 2022.
- [26] Julian Schrittwieser, Ioannis Antonoglou, Thomas Hubert, Karen Simonyan, Laurent Sifre, Simon Schmitt, Arthur Guez, Edward Lockhart, Demis Hassabis, Thore Graepel, et al. Mastering atari, go, chess and shogi by planning with a learned model. *Nature*, 588(7839):604–609, 2020.
- [27] Junhyuk Oh, Xiaoxiao Guo, Honglak Lee, Richard L Lewis, and Satinder Singh. Action-conditional video prediction using deep networks in atari games. *Advances in neural information processing systems*, 28, 2015.
- [28] Łukasz Kaiser, Mohammad Babaeizadeh, Piotr Miłoś, Błażej Osipiński, Roy H Campbell, Konrad Czechowski, Dumitru Erhan, Chelsea Finn, Piotr Kozakowski, Sergey Levine, et al. Model based reinforcement learning for atari. In *International Conference on Learning Representations*, 2020.
- [29] Russell Mendonca, Shikhar Bahl, and Deepak Pathak. Structured world models from human videos. In *Robotics: Science and Systems XIX, Daegu, Republic of Korea, July 10-14, 2023*, 2023.
- [30] Jialong Wu, Haoyu Ma, Chaoyi Deng, and Mingsheng Long. Pre-training contextualized world models with in-the-wild videos for reinforcement learning. *Advances in Neural Information Processing Systems*, 36, 2023.
- [31] Ruben Villegas, Arkanath Pathak, Harini Kannan, Dumitru Erhan, Quoc V Le, and Honglak Lee. High fidelity video prediction with large stochastic recurrent neural networks. *Advances in Neural Information Processing Systems*, 32, 2019.
- [32] Mohammad Babaeizadeh, Mohammad Taghi Saffar, Suraj Nair, Sergey Levine, Chelsea Finn, and Dumitru Erhan. Fitvid: Overfitting in pixel-level video prediction. *arXiv preprint arXiv:2106.13195*, 2021.
- [33] Vikram Voleti, Alexia Jolicoeur-Martineau, and Chris Pal. Mcvd-masked conditional video diffusion for prediction, generation, and interpolation. *Advances in neural information processing systems*, 35:23371–23385, 2022.
- [34] Zheng Zhu, Xiaofeng Wang, Wangbo Zhao, Chen Min, Nianchen Deng, Min Dou, Yuqi Wang, Botian Shi, Kai Wang, Chi Zhang, et al. Is sora a world simulator? a comprehensive survey on general world models and beyond. *arXiv preprint arXiv:2405.03520*, 2024.
- [35] Agrim Gupta, Stephen Tian, Yunzhi Zhang, Jiajun Wu, Roberto Martín-Martín, and Li Fei-Fei. Maskvit: Masked visual pre-training for video prediction. In *ICLR*, 2023.
- [36] Jialong Wu, Shaofeng Yin, Ningya Feng, Xu He, Dong Li, Jianye Hao, and Mingsheng Long. iVideoGPT: Interactive VideoGPTs are scalable world models. *arXiv preprint arXiv:2405.15223*, 2024.
- [37] Tian Xu, Ziniu Li, and Yang Yu. Error bounds of imitating policies and environments for reinforcement learning. *IEEE Transactions on Pattern Analysis and Machine Intelligence*, 44(10):6968–6980, 2022.
- [38] Nathan Lambert, Kristofer Pister, and Roberto Calandra. Investigating compounding prediction errors in learned dynamics models. *arXiv preprint arXiv:2203.09637*, 2022.
- [39] Kavosh Asadi, Dipendra Misra, Seungchan Kim, and Michel L Littman. Combating the compounding-error problem with a multi-step model. *arXiv preprint arXiv:1905.13320*, 2019.

- [40] Haoxin Lin, Yu-Yan Xu, Yihao Sun, Zhilong Zhang, Yi-Chen Li, Chengxing Jia, Junyin Ye, Jiaji Zhang, and Yang Yu. Any-step dynamics model improves future predictions for online and offline reinforcement learning. *arXiv preprint arXiv:2405.17031*, 2024.
- [41] Benjamin Eysenbach, Alexander Khazatsky, Sergey Levine, and Russ R Salakhutdinov. Mismatched no more: Joint model-policy optimization for model-based rl. *Advances in Neural Information Processing Systems*, 35:23230–23243, 2022.
- [42] Raj Ghugare, Homanga Bharadhwaj, Benjamin Eysenbach, Sergey Levine, and Ruslan Salakhutdinov. Simplifying model-based rl: learning representations, latent-space models, and policies with one objective. *arXiv preprint arXiv:2209.08466*, 2022.
- [43] Fan-Ming Luo, Tian Xu, Xingchen Cao, and Yang Yu. Reward-consistent dynamics models are strongly generalizable for offline reinforcement learning. In *The Twelfth International Conference on Learning Representations*, 2024.
- [44] Ruifeng Chen, Chengxing Jia, Zefang Huang, Tian-Shuo Liu, Xu-Hui Liu, and Yang Yu. Offline transition modeling via contrastive energy learning. In *Forty-first International Conference on Machine Learning*, 2024.
- [45] Ying Jin, Zhuoran Yang, and Zhaoran Wang. Is pessimism provably efficient for offline rl? In *International Conference on Machine Learning*, pages 5084–5096. PMLR, 2021.
- [46] Rahul Kidambi, Aravind Rajeswaran, Praneeth Netrapalli, and Thorsten Joachims. Morel: Model-based offline reinforcement learning. In *Advances in Neural Information Processing Systems 33 (NeurIPS’20)*, virtual event, 2020.
- [47] Cong Lu, Philip Ball, Jack Parker-Holder, Michael Osborne, and Stephen J Roberts. Revisiting design choices in offline model based reinforcement learning. In *International Conference on Learning Representations*, 2022.
- [48] Rafael Rafailov, Tianhe Yu, Aravind Rajeswaran, and Chelsea Finn. Offline reinforcement learning from images with latent space models. In *Learning for dynamics and control*, pages 1154–1168. PMLR, 2021.
- [49] Saurav Kadavath, Tom Conerly, Amanda Askell, Tom Henighan, Dawn Drain, Ethan Perez, Nicholas Schiefer, Zac Hatfield-Dodds, Nova DasSarma, Eli Tran-Johnson, et al. Language models (mostly) know what they know. *arXiv preprint arXiv:2207.05221*, 2022.
- [50] Lorenz Kuhn, Yarin Gal, and Sebastian Farquhar. Semantic uncertainty: Linguistic invariances for uncertainty estimation in natural language generation. *arXiv preprint arXiv:2302.09664*, 2023.
- [51] Martin L Puterman. Markov decision processes. *Handbooks in operations research and management science*, 2:331–434, 1990.
- [52] Martin L Puterman. *Markov decision processes: discrete stochastic dynamic programming*. John Wiley & Sons, 2014.
- [53] Richard S Sutton and Andrew G Barto. *Reinforcement learning: An introduction*. MIT press, 2018.
- [54] Siddharth Venkatraman, Shivesh Khaitan, Ravi Tej Akella, John Dolan, Jeff Schneider, and Glen Berseth. Reasoning with latent diffusion in offline reinforcement learning. In *The Twelfth International Conference on Learning Representations, ICLR 2024, Vienna, Austria, May 7-11, 2024*, 2024.
- [55] Yiqin Yang, Hao Hu, Wenzhe Li, Siyuan Li, Jun Yang, Qianchuan Zhao, and Chongjie Zhang. Flow to control: Offline reinforcement learning with lossless primitive discovery. In *Proceedings of the AAAI Conference on Artificial Intelligence*, volume 37, pages 10843–10851, 2023.
- [56] Anurag Ajay, Aviral Kumar, Pulkit Agrawal, Sergey Levine, and Ofir Nachum. OPAL: offline primitive discovery for accelerating offline reinforcement learning. In *9th International Conference on Learning Representations, ICLR 2021, Virtual Event, Austria, May 3-7, 2021*, 2021.
- [57] Irina Higgins, Loic Matthey, Arka Pal, Christopher Burgess, Xavier Glorot, Matthew Botvinick, Shakir Mohamed, and Alexander Lerchner. beta-VAE: Learning basic visual concepts with a constrained variational framework. In *International Conference on Learning Representations*, 2017.
- [58] Haoxin Lin, Yu-Yan Xu, Yihao Sun, Zhilong Zhang, Yi-Chen Li, Chengxing Jia, Junyin Ye, Jiaji Zhang, and Yang Yu. Any-step dynamics model improves future predictions for online and offline reinforcement learning, 2024.
- [59] Aaron Van Den Oord, Oriol Vinyals, et al. Neural discrete representation learning. *Advances in neural information processing systems*, 30, 2017.
- [60] Moo Jin Kim, Karl Pertsch, Siddharth Karamcheti, Ted Xiao, Ashwin Balakrishna, Suraj Nair, Rafael Rafailov, Ethan Paul Foster, Grace Lam, Pannag Sanketi, Quan Vuong, Thomas Kollar, Benjamin Burchfiel, Russ Tedrake, Dorsa Sadigh, Sergey Levine, Percy Liang, and Chelsea Finn. Openvla: An open-source vision-language-action model. *CoRR*, abs/2406.09246, 2024.

- [61] Thomas Unterthiner, Sjoerd Van Steenkiste, Karol Kurach, Raphael Marinier, Marcin Michalski, and Sylvain Gelly. Towards accurate generative models of video: A new metric & challenges. *arXiv preprint arXiv:1812.01717*, 2018.
- [62] Quan Huynh-Thu and Mohammed Ghanbari. Scope of validity of psnr in image/video quality assessment. *Electronics letters*, 44(13):800–801, 2008.
- [63] Richard Zhang, Phillip Isola, Alexei A Efros, Eli Shechtman, and Oliver Wang. The unreasonable effectiveness of deep features as a perceptual metric. In *Proceedings of the IEEE conference on computer vision and pattern recognition*, pages 586–595, 2018.
- [64] Zhou Wang, Alan C Bovik, Hamid R Sheikh, and Eero P Simoncelli. Image quality assessment: from error visibility to structural similarity. *IEEE transactions on image processing*, 13(4):600–612, 2004.
- [65] Tianhe Yu, Garrett Thomas, Lantao Yu, Stefano Ermon, James Y Zou, Sergey Levine, Chelsea Finn, and Tengyu Ma. Mopo: Model-based offline policy optimization. *Advances in Neural Information Processing Systems*, 33:14129–14142, 2020.
- [66] Josh Achiam, Steven Adler, Sandhini Agarwal, Lama Ahmad, Ilge Akkaya, Florencia Leoni Aleman, Diogo Almeida, Janko Altschmidt, Sam Altman, Shyamal Anadkat, et al. Gpt-4 technical report. *arXiv preprint arXiv:2303.08774*, 2023.
- [67] Laurens Van der Maaten and Geoffrey Hinton. Visualizing data using t-sne. *Journal of machine learning research*, 9(11), 2008.
- [68] Stephen Tian, Chelsea Finn, and Jiajun Wu. A control-centric benchmark for video prediction. *arXiv preprint arXiv:2304.13723*, 2023.
- [69] Anthony Brohan, Noah Brown, Justice Carbajal, Yevgen Chebotar, Joseph Dabis, Chelsea Finn, Keerthana Gopalakrishnan, Karol Hausman, Alex Herzog, Jasmine Hsu, et al. Rt-1: Robotics transformer for real-world control at scale. *arXiv preprint arXiv:2212.06817*, 2022.
- [70] Dmitry Kalashnikov, Alex Irpan, Peter Pastor, Julian Ibarz, Alexander Herzog, Eric Jang, Deirdre Quillen, Ethan Holly, Mrinal Kalakrishnan, Vincent Vanhoucke, et al. QT-Opt: Scalable deep reinforcement learning for vision-based robotic manipulation. *arXiv preprint arXiv:1806.10293*, 2018.
- [71] Frederik Ebert, Yanlai Yang, Karl Schmeckpeper, Bernadette Bucher, Georgios Georgakis, Kostas Daniilidis, Chelsea Finn, and Sergey Levine. Bridge data: Boosting generalization of robotic skills with cross-domain datasets. *arXiv preprint arXiv:2109.13396*, 2021.
- [72] Homer Walke, Kevin Black, Abraham Lee, Moo Jin Kim, Max Du, Chongyi Zheng, Tony Zhao, Philippe Hansen-Estruch, Quan Vuong, Andre He, Vivek Myers, Kuan Fang, Chelsea Finn, and Sergey Levine. Bridgedata v2: A dataset for robot learning at scale, 2023.
- [73] Erick Rosete-Beas, Oier Mees, Gabriel Kalweit, Joschka Boedecker, and Wolfram Burgard. Latent plans for task agnostic offline reinforcement learning. In *Proceedings of the 6th Conference on Robot Learning (CoRL)*, 2022.
- [74] Oier Mees, Jessica Borja-Diaz, and Wolfram Burgard. Grounding language with visual affordances over unstructured data. In *Proceedings of the IEEE International Conference on Robotics and Automation (ICRA)*, London, UK, 2023.
- [75] Shivin Dass, Jullian Yapeter, Jesse Zhang, Jiahui Zhang, Karl Pertsch, Stefanos Nikolaidis, and Joseph J. Lim. CLVR jaco play dataset, 2023.
- [76] Jianlan Luo, Charles Xu, Xinyang Geng, Gilbert Feng, Kuan Fang, Liam Tan, Stefan Schaal, and Sergey Levine. Multi-stage cable routing through hierarchical imitation learning. *arXiv preprint arXiv:2307.08927*, 2023.
- [77] Ajay Mandlekar, Yuke Zhu, Animesh Garg, Jonathan Boother, Max Spero, Albert Tung, Julian Gao, John Emmons, Anchit Gupta, Emre Orbay, Silvio Savarese, and Li Fei-Fei. RoboTurk: A crowdsourcing platform for robotic skill learning through imitation. *CoRR*, abs/1811.02790, 2018.
- [78] Yifeng Zhu, Abhishek Joshi, Peter Stone, and Yuke Zhu. Viola: Imitation learning for vision-based manipulation with object proposal priors, 2023.
- [79] Lawrence Yunliang Chen, Simeon Adebola, and Ken Goldberg. Berkeley UR5 demonstration dataset. <https://sites.google.com/view/berkeley-ur5/home>.
- [80] Gaoyue Zhou, Victoria Dean, Mohan Kumar Srirama, Aravind Rajeswaran, Jyothish Pari, Kyle Hatch, Aryan Jain, Tianhe Yu, Pieter Abbeel, Lerrel Pinto, Chelsea Finn, and Abhinav Gupta. Train offline, test online: A real robot learning benchmark, 2023.

- [81] Corey Lynch, Ayzaan Wahid, Jonathan Tompson, Tianli Ding, James Betker, Robert Baruch, Travis Armstrong, and Pete Florence. Interactive language: Talking to robots in real time. *IEEE Robotics and Automation Letters*, 2023.
- [82] Suneel Belkhale, Yuchen Cui, and Dorsa Sadigh. Hydra: Hybrid robot actions for imitation learning. *arxiv*, 2023.
- [83] Yifeng Zhu, Peter Stone, and Yuke Zhu. Bottom-up skill discovery from unsegmented demonstrations for long-horizon robot manipulation. *IEEE Robotics and Automation Letters*, 7(2):4126–4133, 2022.
- [84] Zichen Jeff Cui, Yibin Wang, Nur Muhammad Mahi Shafiullah, and Lerrel Pinto. From play to policy: Conditional behavior generation from uncured robot data. *arXiv preprint arXiv:2210.10047*, 2022.
- [85] Minh Heo, Youngwoon Lee, Doohyun Lee, and Joseph J. Lim. Furniturebench: Reproducible real-world benchmark for long-horizon complex manipulation. In *Robotics: Science and Systems*, 2023.
- [86] Ge Yan, Kris Wu, and Xiaolong Wang. ucsd kitchens Dataset. August 2023.
- [87] Soroush Nasiriany, Tian Gao, Ajay Mandlekar, and Yuke Zhu. Learning and retrieval from prior data for skill-based imitation learning. In *Conference on Robot Learning (CoRL)*, 2022.
- [88] Huihan Liu, Soroush Nasiriany, Lance Zhang, Zhiyao Bao, and Yuke Zhu. Robot learning on the job: Human-in-the-loop autonomy and learning during deployment. In *Robotics: Science and Systems (RSS)*, 2023.
- [89] Gabriel Quere, Annette Hagengruber, Maged Iskandar, Samuel Bustamante, Daniel Leidner, Freek Stulp, and Joern Vogel. Shared Control Templates for Assistive Robotics. In *2020 IEEE International Conference on Robotics and Automation (ICRA)*, page 7, Paris, France, 2020.
- [90] Saumya Saxena, Mohit Sharma, and Oliver Kroemer. Multi-resolution sensing for real-time control with vision-language models. In *7th Annual Conference on Robot Learning*, 2023.
- [91] Rutav Shah, Roberto Martín-Martín, and Yuke Zhu. MUTEX: Learning unified policies from multimodal task specifications. In *7th Annual Conference on Robot Learning*, 2023.
- [92] Xinghao Zhu, Ran Tian, Chenfeng Xu, Mingyu Ding, Wei Zhan, and Masayoshi Tomizuka. Fanuc manipulation: A dataset for learning-based manipulation with fanuc mate 200id robot. 2023.
- [93] Russell Mendonca, Shikhar Bahl, and Deepak Pathak. Structured world models from human videos. *CoRL*, 2023.
- [94] Eric Jang, Alex Irpan, Mohi Khansari, Daniel Kappler, Frederik Ebert, Corey Lynch, Sergey Levine, and Chelsea Finn. Bc-z: Zero-shot task generalization with robotic imitation learning. In *Conference on Robot Learning*, pages 991–1002. PMLR, 2022.
- [95] Jianlan Luo, Charles Xu, Fangchen Liu, Liam Tan, Zipeng Lin, Jeffrey Wu, Pieter Abbeel, and Sergey Levine. Fmb: a functional manipulation benchmark for generalizable robotic learning. *arXiv preprint arXiv:2401.08553*, 2024.
- [96] Nur Muhammad Mahi Shafiullah, Anant Rai, Haritheja Etukuru, Yiqian Liu, Ishan Misra, Soumith Chintala, and Lerrel Pinto. On bringing robots home, 2023.
- [97] Alexander Khazatsky, Karl Pertsch, Suraj Nair, Ashwin Balakrishna, Sudeep Dasari, Siddharth Karamcheti, Soroush Nasiriany, Mohan Kumar Srirama, Lawrence Yunliang Chen, Kirsty Ellis, et al. Droid: A large-scale in-the-wild robot manipulation dataset. *arXiv preprint arXiv:2403.12945*, 2024.
- [98] Zipeng Fu, Tony Z Zhao, and Chelsea Finn. Mobile aloha: Learning bimanual mobile manipulation with low-cost whole-body teleoperation. *arXiv preprint arXiv:2401.02117*, 2024.
- [99] Laurens Van der Maaten and Geoffrey Hinton. Visualizing data using t-sne. *Journal of machine learning research*, 9(11), 2008.

A Analysis of behavior-conditioning

In this section, we provide some theoretical explanations about why behavior-conditioning mechanism helps mitigate the generalization error caused by the policy divergence. The analysis is mainly adapted from [9].

First, we introduce an assumption on the smoothness of a well-trained dynamics model:

Assumption A.1 *For the learned dynamics model T , the point-wise total-variation model error $D_{\text{TV}}[T^*(\cdot|\tau_h), T(\cdot|\tau_h)]$ is L -Lipschitz with respect to the trajectory inputs, i.e.,*

$$\left| D_{\text{TV}}[T^*(\cdot|\tau_h^1), T(\cdot|\tau_h^1)] - D_{\text{TV}}[T^*(\cdot|\tau_h^2), T(\cdot|\tau_h^2)] \right| \leq L \cdot D(\tau_h^1, \tau_h^2),$$

where $D(\cdot, \cdot)$ is some kind of distance defined on the trajectory space.

Assumption A.1 measures the local extrapolation ability of a world model. Based on this assumption, the value gaps of common dynamics model T without a behavior-conditioning mechanism can be controlled:

Proposition A.2 *Under Assumption A.1, for any policy π , the value gap of common dynamics model T without behavior-conditioning has an upper bound:*

$$\left| V_T^\pi - V_{T^*}^\pi \right| \leq 2R_{\max} H^2 \left(\underbrace{\sqrt{2 l_{\text{KL}}(T; \Pi)}}_{\text{in distribution error}} + \underbrace{L \cdot W_1(d^\pi, d^\Pi)}_{\text{policy divergence}} \right),$$

where $W_1(d^\pi, d^\Pi)$ is the Wasserstein-1 distance between the π -induced trajectory distribution $d^\pi(\tau)$ and the behavior trajectory distribution $d^\Pi(\tau) = \mathbb{E}_{\mu \sim \Pi}[d^\mu(\tau)]$.

Proposition A.2 shows that the generalization of common dynamics model T solely relies on its point-level smoothness over the trajectory inputs, resulting in an inevitable extrapolation error of the policy distribution. In contrast, a policy-conditioned dynamics model $T(\cdot)$, which yields adapted dynamics model $T(\pi)$ for some policy π , takes a further step to reduce the policy distribution extrapolation error:

Proposition A.3 *Under Assumption A.1, for any policy π , the value gap of policy-conditioned dynamics model $T(\cdot)$ has an upper bound:*

$$\left| V_{T(\pi)}^\pi - V_{T^*}^\pi \right| \leq 2R_{\max} H^2 \left(\underbrace{\sqrt{2 l_{\text{KL}}(T; \Pi)}}_{\text{in distribution error}} + \underbrace{L \cdot W_1(d^\pi, d^\Pi) - C(\pi, \Pi)}_{\text{reduced policy divergence}} \right),$$

where the adaptation gain $C(\pi, \Pi) := \mathbb{E}_{\mu \sim \Pi} \mathbb{E}_{\tau \sim d^\pi} D_{\text{TV}}[T^*, T(\mu)](\tau) - \mathbb{E}_{\tau \sim d^\pi} D_{\text{TV}}[T^*, T(\pi)](\tau)$ summarizes the policy adaptation effect.

Proposition A.3 explains the benefit brought by behavior-conditioning: a positive adaptation gain $C(\pi, \Pi)$, which quantifies the advantage of the policy adaptation effect. The key insight is that when testing on an unseen policy π within some effective region, the model $T(\pi)$, customized for π , should exhibit a smaller model error under the target trajectory distribution d^π compared to models $T(\mu)$ trained on behavior policies $\mu \in \Pi$, which mitigates the generalization error caused by the policy extrapolation. Although it is challenging to rigorously analyze the adaptation gain $C(\pi, \Pi)$ due to the complexity of neural networks and the optimization process, qualitative discussions and empirical evidence, as shown in [9], justify the underlying rationale.

B Implementation Details

B.1 Implementation Details of Whale-ST and Whale-X

Video Tokenizer. Here we show the architecture and training hyperparameter of the video tokenizer as shown in Table 5. We train three different video tokenizers in total.

Behavior-conditioning Model. The model architecture and training hyperparameters of the behavior-conditioning model are shown in Table 6. We also train three different behavior embedding models for Whale-ST and Whale-X. Additionally, We also observe overfitting in the behavior-conditioning model during pre-training, prompting the use of the early-stop technique. As a result, the checkpoint at 50k is selected as the final model for Whale-X.

Component	Parameter	Whale-ST _(64×64)	Whale-ST _(256×256)	Whale-X _(256×256)
Encoder	num_layers	4	12	12
	d_model	512	512	512
	num_heads	8	8	8
Decoder	num_layers	8	16	20
	d_model	512	512	1024
	num_heads	8	8	16
Codebook	num_codes	1024	1024	2048
	patch_size	4	16	16
	latent_dim	32	32	32
	beta	0.25	0.25	0.25
Optimizer	type	AdamW	AdamW	AdamW
	max_lr	3e-4	3e-4	3e-4
	min_lr	3e-4	3e-4	3e-5
	β_1	0.9	0.9	0.9
	β_2	0.9	0.9	0.9
	weight_decay	1e-4	1e-4	0
	warmup_steps	10k	10k	5k
	batch_size	32	32	64
	training_steps	100k	150k	300k

Table 5: Hyperparameter of video tokenizers.

Component	Parameter	Whale-ST _(64×64)	Whale-ST _(256×256)	Whale-X _(256×256)
Posterior	num_layers	8	8	12
	d_model	512	512	768
	num_heads	8	8	12
	patch_size	8	32	32
Prior	num_layers	4	4	8
	d_model	512	512	512
	num_heads	4	4	8
	patch_size	8	32	32
Policy	num_layers	8	8	12
	d_model	512	512	768
	num_heads	8	8	12
	log_std	[-2, 5]	[-2, 5]	[-2, 5]
	patch_size	8	32	32
Embedding	category_size	16	16	16
	class_size	16	16	16
Optimizer	type	AdamW	AdamW	AdamW
	max_lr	3e-4	3e-4	3e-4
	min_lr	3e-5	3e-5	3e-5
	β_1	0.9	0.9	0.9
	β_2	0.9	0.9	0.9
	weight_decay	1e-4	1e-4	1e-4
	warmup_steps	5k	5k	5k
	batch_size	64	64	64
	training_steps	100k	100k	50k

Table 6: Hyperparameter of behavior-conditioning models.

Model	#Parameters (dynamics only)	num_layers	num_heads	d_model
Whale-ST (64)	26M	12	8	512
Whale-ST (256)	26M	12	8	512
Whale-X-small	39M	18	8	512
Whale-X-medium	77M	16	16	768
Whale-X-base	204M	24	16	1024
Whale-X-large	456M	24	12	1536

Table 7: Model hyperparameter of dynamics models.

Parameter	Value
max_lr	3e-5
min_lr	3e-6
β_1	0.9
β_2	0.9
weight_decay	0
warmup_steps	5k
batch_size	64
training_steps	300k

Table 8: Trainig hyperparameter of dynamics models.

Dynamics model Table 7 and Table 8 present the hyperparameters of the dynamics model. We train a total of 6 different dynamics models. The architecture design and training hyperparameters of our dynamics model are also referred to [11].

B.2 Fine-tuning Details of Whale-X

For fine-tuning all pre-trained models, we first update the video tokenizer for 5000 gradient steps while keeping the encoder network fixed. After that, we update the behavior-conditioning model for 1000 gradient steps, and finally, we update the dynamics model for 5000 gradient steps. For training models from scratch, the video tokenizer, behavior-conditioning model, and dynamics model are all updated for 10,000 gradient steps.

B.3 Implementation Details of Baselines

Baselines for model evaluation We use the official implementation of VP2 [68] for both FitVid and MCVD. For DreamerV3, we retain only the world model learning component. Additionally, we use the official implementation of iVideoGPT as described in their original paper, but with a reduced number of parameters. The detailed hyperparameters for DreamerV3 and iVideoGPT are provided in Table 9 and Table 10, respectively.

Baselines for uncertainty estimation We implement both entropy-based and ensemble-based uncertainty estimation methods based on Whale-ST. The entropy-based method directly uses the entropy of the logits output by the dynamics model as the measure of uncertainty. For the ensemble-based method, we independently train three dynamics models and use the pixel-level variance between their output images as the measure of uncertainty.

B.4 Implementation Details of Evaluation Metrics

Evaluation metrics for model evaluation The metrics we use for model evaluation are defined as follows:

Absolute Error The absolute error is defined as the difference between the value and estimated value of a policy:

$$\text{AbsErr} = |V^\pi - \hat{V}^\pi|, \quad (7)$$

where V^π is the true value of the policy and \hat{V}^π is the estimated value of the policy.

Hyperparameters	Values
# Parameters	44M
Dynamics hidden	1024
Dynamics deterministic	1024
Dynamics stochastic	32
Dynamics discrete	32
CNN depth	64
CNN kernel size	4
MLP layers	5
MLP units	1024
Actionvation	SiLU
Train batch size	32
Train batch length	8

Table 9: Hyperparameters for DreamerV3.

Hyperparameters	Values
# Parameters	63M
Down blocks	3
Down layers per block	2
Down channels	[64, 128, 256]
Up blocks	3
Up layers per block	3
Up channels	[256, 128, 64]
Embedding dim	64
Codebook size	8192
Actionvation	SiLU
Transformer hidden dim	512
Transformer hidden layers	6
Attention Heads	8
Feedforward dim	1024

Table 10: Hyperparameters for iVideoGPT.

Rank correlation Rank correlation measures the correlation between the ordinal rankings of the value estimates and the true values, which can be written as:

$$\text{RankCorr} = \frac{\text{Cov}(V_{1:N}^\pi, \hat{V}_{1:N}^\pi)}{\sigma(V_{1:N}^\pi)\sigma(\hat{V}_{1:N}^\pi)}, \quad (8)$$

where $1 : N$ denotes the indices of the evaluated policies.

Regret@k Regret@k is the difference between the value of the best policy in the entire set, and the value of the best policy in the top-k set (where the top-k set is chosen by estimated values). It can be defined as:

$$\text{Regret @k} = \max_{i \in 1:N} V_i^\pi - \max_{j \in \text{topk}(1:N)} V_j^\pi, \quad (9)$$

where $\text{topk}(1 : N)$ denotes the indices of the top K policies as measured by estimated values \hat{V}^π .

Evaluation metrics for uncertainty estimation For model error prediction, we use unseen action sequences to rollout 8 steps in Whale-ST, and measure model error using the perceptual loss between the generated samples and the real samples. For offline MBRL evaluation, Figure 4 shows the success rate over gradient update steps of different uncertainty estimation algorithms across five different tasks. For each evaluation, we sample 20 trajectories to calculate the success rate of the current policy, with a maximum trajectory length truncated at 100. Additionally, we set the uncertainty penalty coefficients as follows: 50 for retracing rollout, 5000 for the ensemble-based method, and 0.1 for the entropy-based method. Additionally, we set the model rollout horizon to 4, the mix ratio of real and generated samples to 0.5, and kept the hyperparameters consistent across all tasks.

C Data Preparation

C.1 Simulated Data

We select a total of 20 tasks from the MetaWorld benchmark. Each task includes a training set of 3,000 trajectories and a test set of 1,500 trajectories. Specifically, for each task, we use six different policies to collect the training set: expert policy, random policy, two suboptimal policies with different levels of Gaussian noise, and two cross-environment policies. Additionally, three unseen policies are used to gather the testing data. The world models are trained on the full training dataset, followed by a thorough evaluation using the testing data.

C.2 Pre-training Data

Follow [60], our pre-training dataset collection includes 27 datasets, with a total scale of 970k demonstrations, as shown in Table 11.

Whale-X Pre-training Dataset Mixture	Percentage
Fractal [69]	12.7%
Kuka [70]	12.7%
Bridge [71, 72]	13.3%
Taco Play [73, 74]	3.0%
Jaco Play [75]	0.4%
Berkeley Cable Routing [76]	0.2%
Roboturk [77]	2.3%
Viola [78]	0.9%
Berkeley Autolab UR5 [79]	1.2%
Toto [80]	2.0%
Language Table [81]	4.4%
Stanford Hydra Dataset [82]	4.4%
Austin Buds Dataset [83]	0.2%
NYU Franka Play Dataset [84]	0.8%
Furniture Bench Dataset [85]	2.4%
UCSD Kitchen Dataset [86]	<0.1%
Austin Sailor Dataset [87]	2.2%
Austin Sirius Dataset [88]	1.7%
DLR EDAN Shared Control [89]	<0.1%
IAMLab CMU Pickup Insert [90]	0.9%
UTAustin Mutex [91]	2.2%
Berkeley Fanuc Manipulation [92]	0.7%
CMU Stretch [93]	0.2%
BC-Z [94]	7.5%
FMB Dataset [95]	7.1%
DobbE [96]	1.4%
DROID [97]	10.0%

Table 11: Whale-X Pre-training Dataset Mixture.

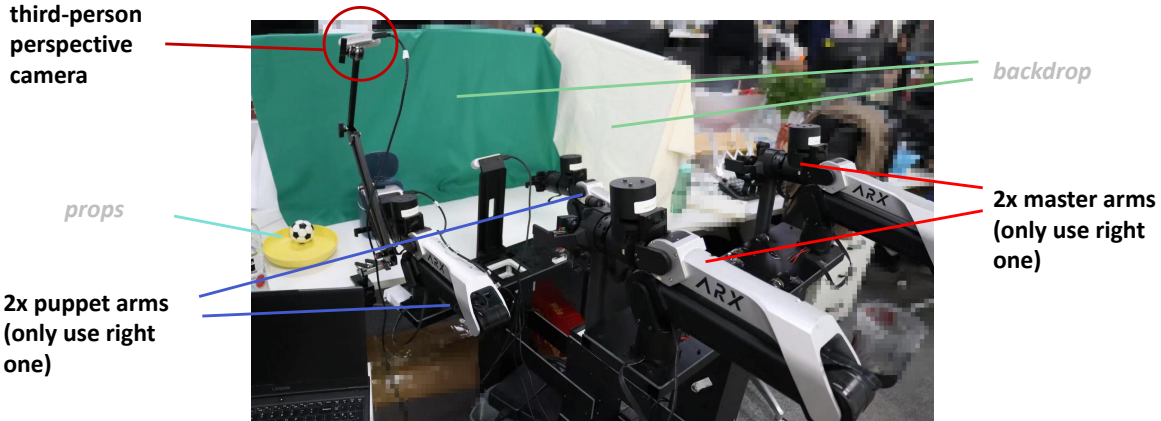


Figure 9: The illustration of our robotics platform used for physical robot evaluation.

D Real-world Task Design

D.1 Hardware Setup

Our hardware setup is shown in Figure 9. For the embodiment, we use the ARX5 robotic platform, which is similar to Aloha [98] and includes two master arms and two puppet arms. Data is collected via teleoperation and we only use the right arm in our experiment. For the vision sensor, a Realsense D435i camera is mounted above the left side of the platform to capture RGB image observations.

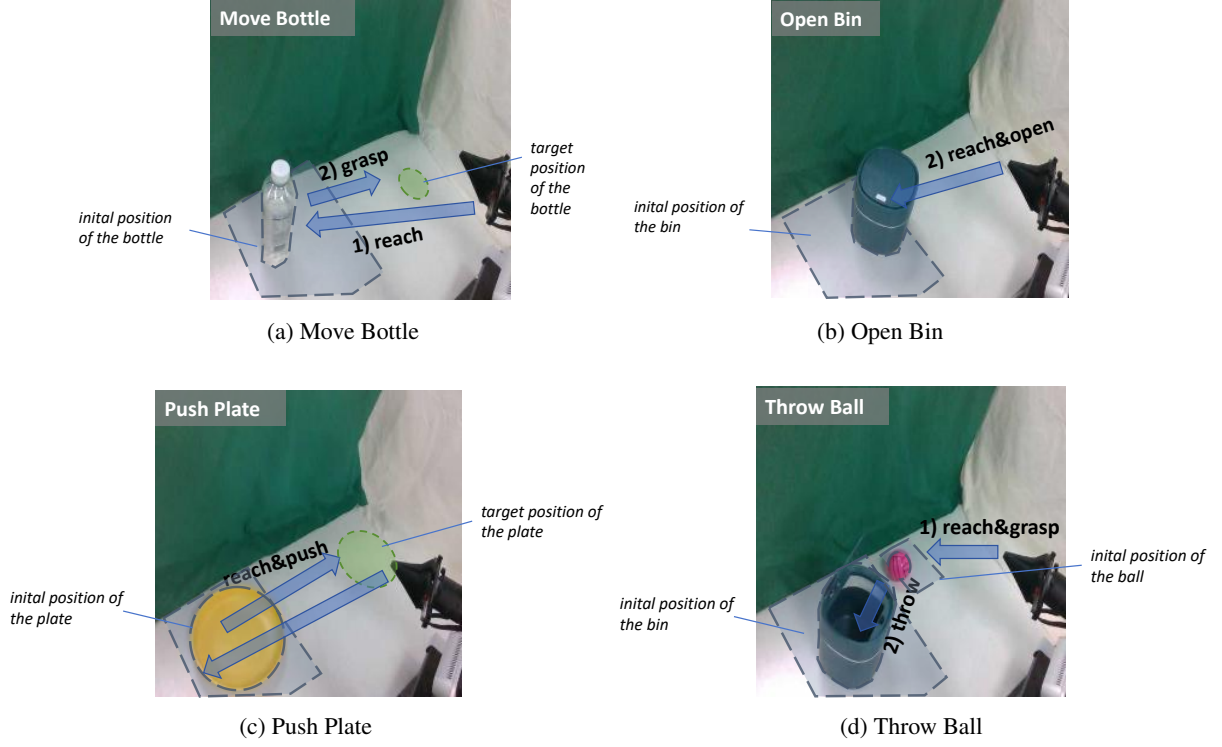


Figure 10: The illustration of Training Tasks.

D.1.1 Details of Tasks

The training data set used for finetuning consists of 4 tasks: **Move Bottle**, **Open Bin**, **Push Plate**, and **Throw Ball**.

Move Bottle: The robot arm must first grasp the bottle and then move it to a specific area on the right side of the table. The bottle’s initial position is somewhat random, varying within a range of two bottle widths around the location shown in the figure, while its target position remains fixed.

Open Bin: In this task, the robot arm must press a small white area on the trash bin’s lid to open it. The initial position of the trash bin has some randomness, and it may vary within a 5 cm range around the position shown in the figure. Additionally, the orientation of the trash bin may have a random variation of about 10 degrees relative to its square alignment.

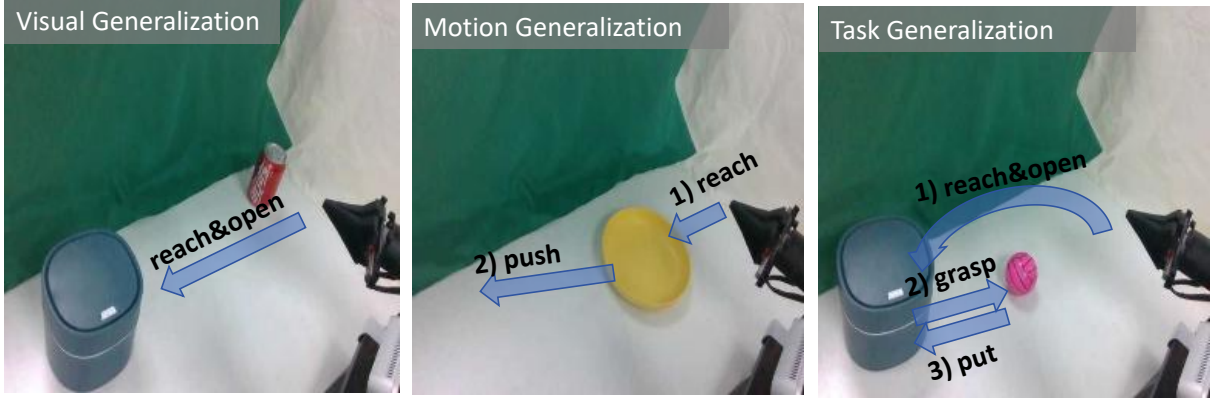
Push Plate: In this task, the robot arm must push the plate from the left side of the table to the right with appropriate force and angle. The challenge lies in the fact that the plate may rotate or shift during the pushing process. The initial position of the plate has some randomness, varying within a 5 cm range around the position shown in the figure. The robot arm needs to push the plate at a distance of approximately 20 cm.

Throw Ball: In this task, the robot arm needs to make a two-stage decision: 1) move to the ball’s location and grasp it; 2) move to the trash bin’s opening and release the gripper. The initial position of the trash bin has some randomness, varying within a 5 cm range around the position shown in the figure.

Visual Generalization: In this unseen scenario, we introduced several visual distractors not encountered during the fine-tuning phase, including a soda can, a plate, a ball, and a pencil, based on the Open Bin task. This task is designed to test the robustness of the world model’s visual representation and its generalization in visual perception.

Motion Generalization: In this unseen scenario, based on the Push Plate task, we changed the specific task from pushing left to right in the fine-tuning data to pushing right to left. This task is designed to evaluate the model’s ability to generalize environment transition modeling when facing an unseen action distribution, or even a completely reversed action distribution.

Task Generalization: In this unseen scenario, we combined two tasks from the fine-tuning phase—Open Bin and Throw Ball—into a new two-stage task. In this task, the robot arm must first open the bin and then place the ball inside. This task is designed to test the model’s generalization ability to new tasks, as well as its capability to model long-horizon actions.



(a) Visual Generalization

(b) Motion Generalization

(c) Task Generalization

Figure 11: The illustration of Generalization Tasks.

D.2 Data Overview

Entry	Value
# Episodes	300(240 for fine-tuning, 60 for testing)
Average horizon	30
Data Collect Method	Human teleoperation using the master arm
Scene Type	Table top
Robot Morphology	Single arm
Camera resolution	640x480
# Cameras	1
Action dimension	7
Action space	EEF position
Action semantics	$(\Delta x, \Delta y, \Delta z, \Delta \text{roll}, \Delta \text{pitch}, \Delta \text{yaw}, \text{the gripper state})$
Control frequency	5Hz
Has suboptimal?	Yes(some failure data for fine-tuning)
Has camera calibration?	No

Table 12: The meta Information of data used in physical robot evaluation.

E Additional Experimental Results

E.1 Qualitative Evaluation

Qualitative Evaluation on Simulated Task Figure 12 shows the results of Whale-ST and baselines after rolling out 64 steps in two different tasks. Notably, this qualitative evaluation is highly challenging and presents significant complexities. First, the evaluation rollout horizon is set to 64, exceeding that used in prior works, which imposes substantial demands on the generalizability and robustness of world models. Moreover, the variations between adjacent frames are subtle in the Meta-World environment, requiring world models to learn the semantics of actions from these minimal changes. In each image, the first row represents the real trajectory, while the others show the generated trajectories. It can be observed that Whale-ST not only generates high-fidelity videos but also accurately restores the robot arm’s pose. DreamerV3 is the baseline closest to Whale, but its generated trajectory still loses key information, such as the blue marker representing the target point. The other baselines fail to accurately model the robot arm’s pose changes from the subtle variations between adjacent frames.

Qualitative Evaluation on Open X-Embodiment Dataset Figure 13 shows the qualitative evaluation results of Whale-X on Open X-Embodiment dataset. Whale-X demonstrates a remarkable ability to generate high-fidelity, action-conditioned trajectories. Moreover, with the aid of retracing-rollout and behavior-conditioning techniques, Whale-X consistently delivers highly accurate predictions of the robotic arm’s pose.

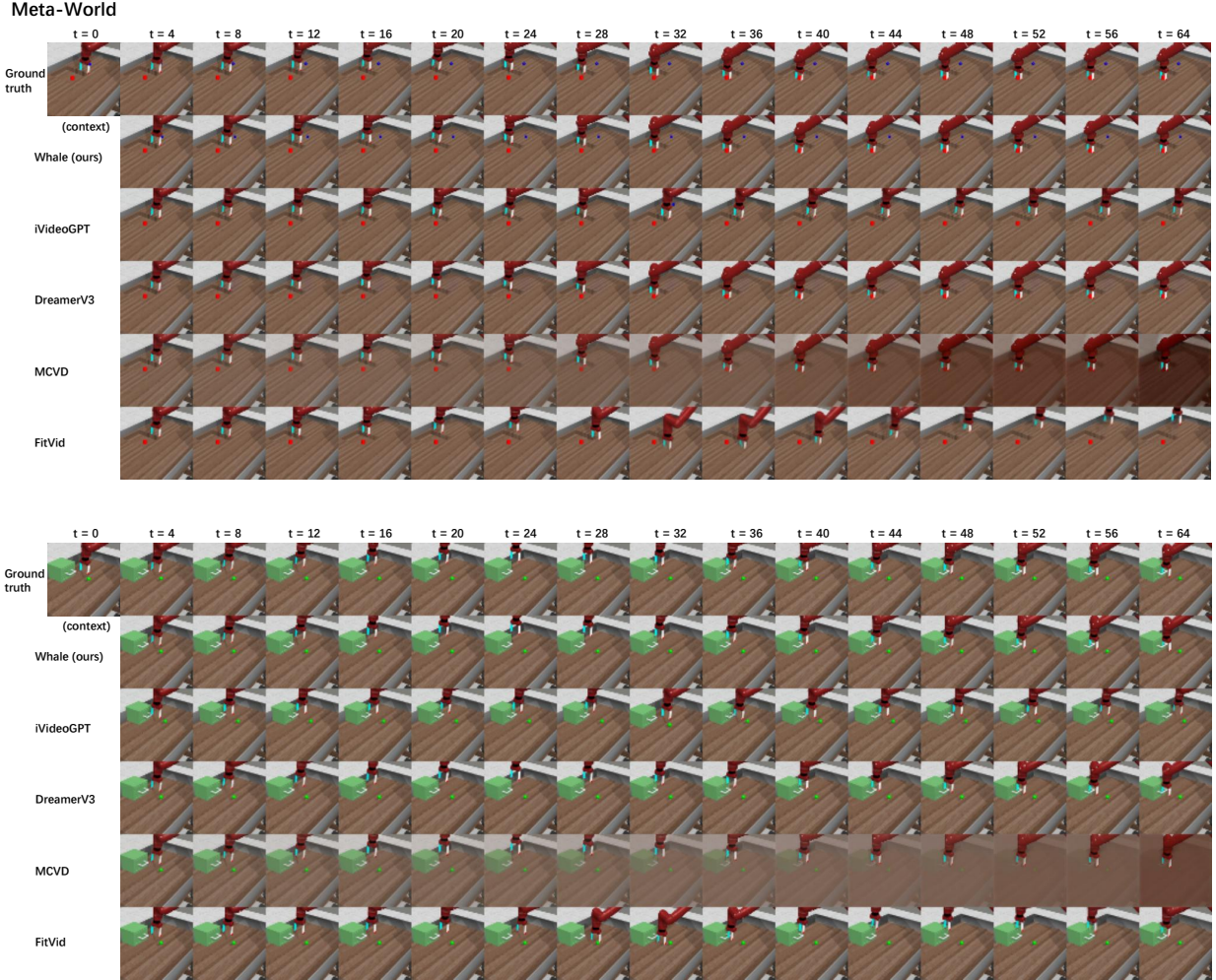


Figure 12: Additional qualitative evaluation on the Meta-World dataset.

Qualitative Evaluation on Real-world Task Figure 14 shows the qualitative evaluation results of Whale-X on Real-world Tasks. Whale-X demonstrates strong generalizability in terms of motion, visualization, and task combination.

E.2 Uncertainty Estimation Visualization

Figure 16 presents model error prediction results across all 20 tasks, illustrating that the retracing-rollout method consistently outperforms both entropy-based and ensemble-based methods in accuracy.

E.3 Behavior Embedding Visualization

Figure 15 shows the visualization results of behavior embedding analysis.

F GPT-4o Evaluation Details

F.1 Q&A Example

We use the large vision language model GPT-4o for evaluation in the physical robot experiment. Generally, we input the real final frame and the model-generated final frame to GPT-4o, using natural language dialogue to enable GPT-4o to assess whether the generated errors in key information such as the robot arm’s position and the status of interactive

objects fall within an acceptable range, thus determining whether the generated results are consistent with reality. Figure 17 shows one of our dialogue examples with GPT-4o. We use multi-turn dialogue to enable the model to easily process and infer information from images.

F.2 All GPT-4o Prompts

Table 13 contains all the prompts we used with GPT-4o for evaluation in unseen scenarios. The prompts evaluate various criteria by listing factors such as the robotic arm’s position and the status of interactive objects.

Task	Prompt
Visual Generalization	Here are two images. The first image is the last frame of a real scene, and I will provide you with another image predicted by a model. The task is to open the trash bin under an unseen background. The trash bin is on the left side of the desk and is closed at the beginning. You need to determine if the two images are consistent based on the following criteria: 1) You can see the inside of the trash bin. 2) Is the predicted image clear? When all these criteria are satisfied, we call the predicted image consistent with the real one. Now I will show you the real image.
Motion Generalization	Here are two images. The first image is the last frame of a real scene, and I will provide you with another image predicted by a model. You need to determine if the two images are consistent based on the following criteria: 1) Is the plate’s position on the left side of the image? 2) Does the plate disappear in the predicted image? 3) Is the predicted image clear? 4) Is the robot arm still present in the predicted image? 5) Does the position of the robot arm in the predicted image match that of the real image? When all these criteria are satisfied, we call the predicted image consistent with the real one. Now I will show you the real image.
Task Generalization	Here are two images. The first image is the last frame of a real scene, and I will provide you with another image predicted by a model. You need to determine if the two images are consistent based on the following criteria: 1) You can see the inside of the trash bin. 2) The ball should be simply missing and not on the desk. 3) Is there any severe distortion in the predicted image? 4) Is the position of the robot arm in the predicted image not far away from that of the real image? When all these criteria are satisfied, we call the predicted image consistent with the real one. Now I will show you the real image.

Table 13: The prompt used for 3 unseen tasks.

F.3 More Evaluation Results

Figure 18 19 20 show the evaluation results for Whale-X, Whale-X (w/o behavior-conditioning), and Whale-X (training from scratch) on the Visual Generalization task. Figure 24 25 26 show the evaluation results for Whale-X, Whale-X (w/o behavior-conditioning), and Whale-X (training from scratch) on the Motion Generalization task. Figure 21 22 23 show the evaluation results for Whale-X, Whale-X (w/o behavior-conditioning), and Whale-X (training from scratch) on the Task Generalization task.

G Computational Resources

Our models for simulated Meta-World tasks are trained and evaluated on a single RTX 4090 GPU platform, while Whale-X for real-world robot manipulation is trained and evaluated using 8 RTX 4090 GPUs. On simulated tasks, it is approximately 2 days for tokenizer training, 8 hours for behavior-conditioning model training, and 1 day for dynamics model training, totaling around 3 days. Pre-training a Whale-X-base model using 8 RTX-4090 GPUs takes about 10 days in total. Specifically, tokenizer training requires 6 days, dynamics model training takes 3 days, and behavior-conditioning model training takes less than 1 day.

Open X-Embodiment



Figure 13: Additional qualitative evaluation on the Open X-Embodiment dataset.

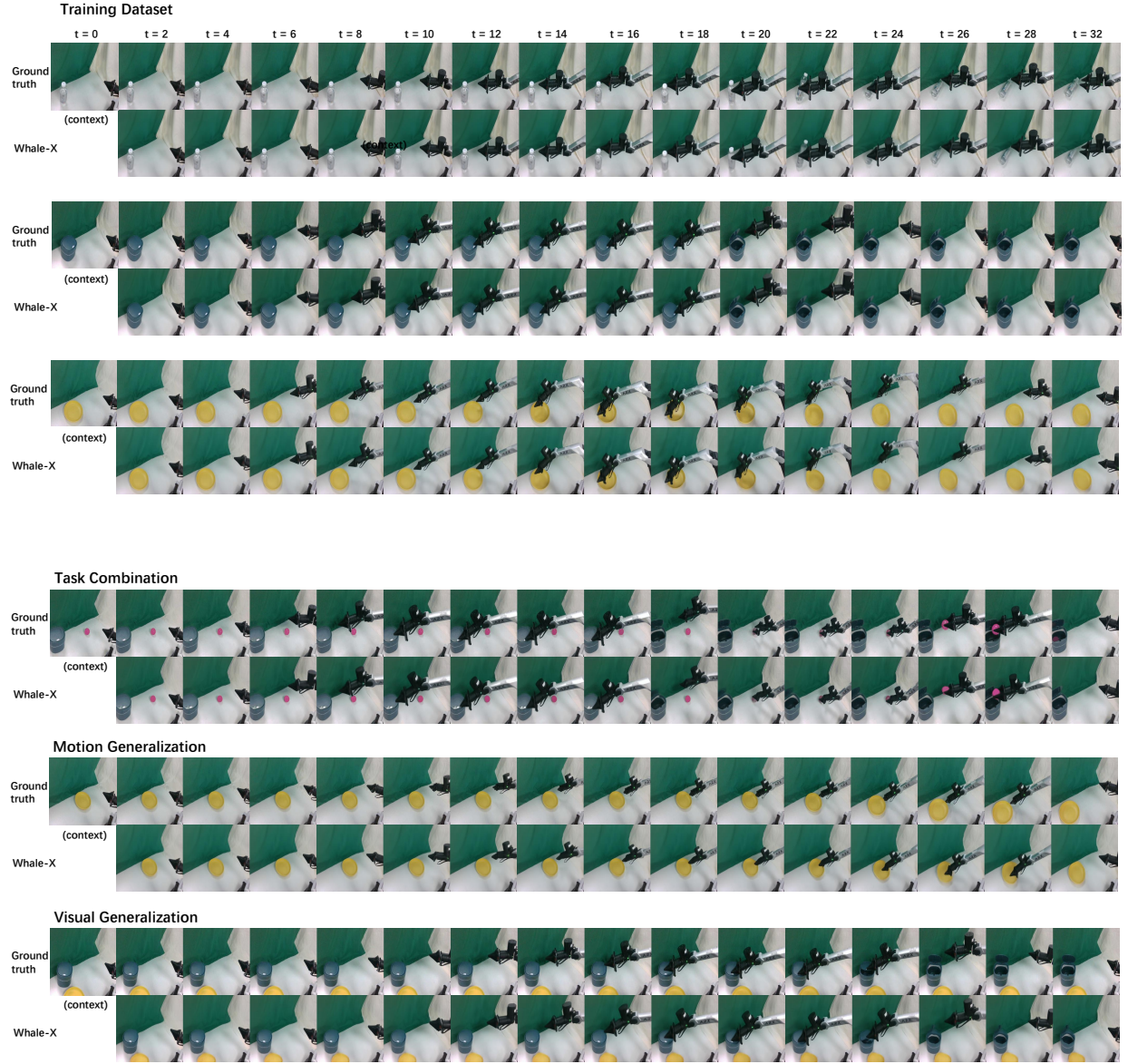


Figure 14: Additional qualitative evaluation on the Real-world tasks.

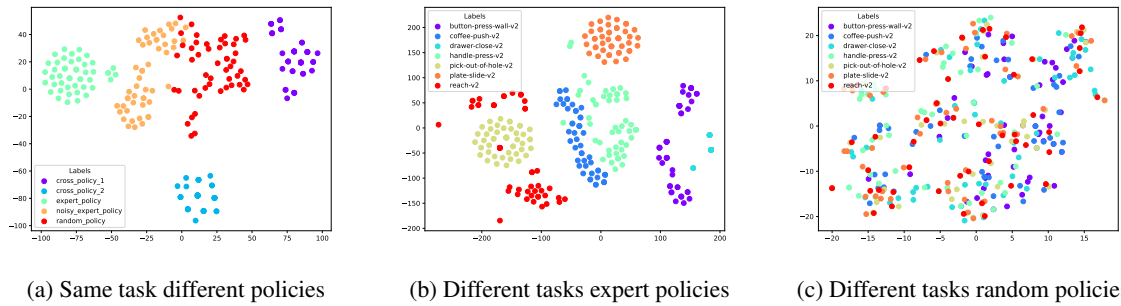


Figure 15: The behavior embedding visualization via t-SNE [99]. The different colors denote different policies in the same task (15a) and expert policies in different tasks (15b) or random policies in different tasks (15c).

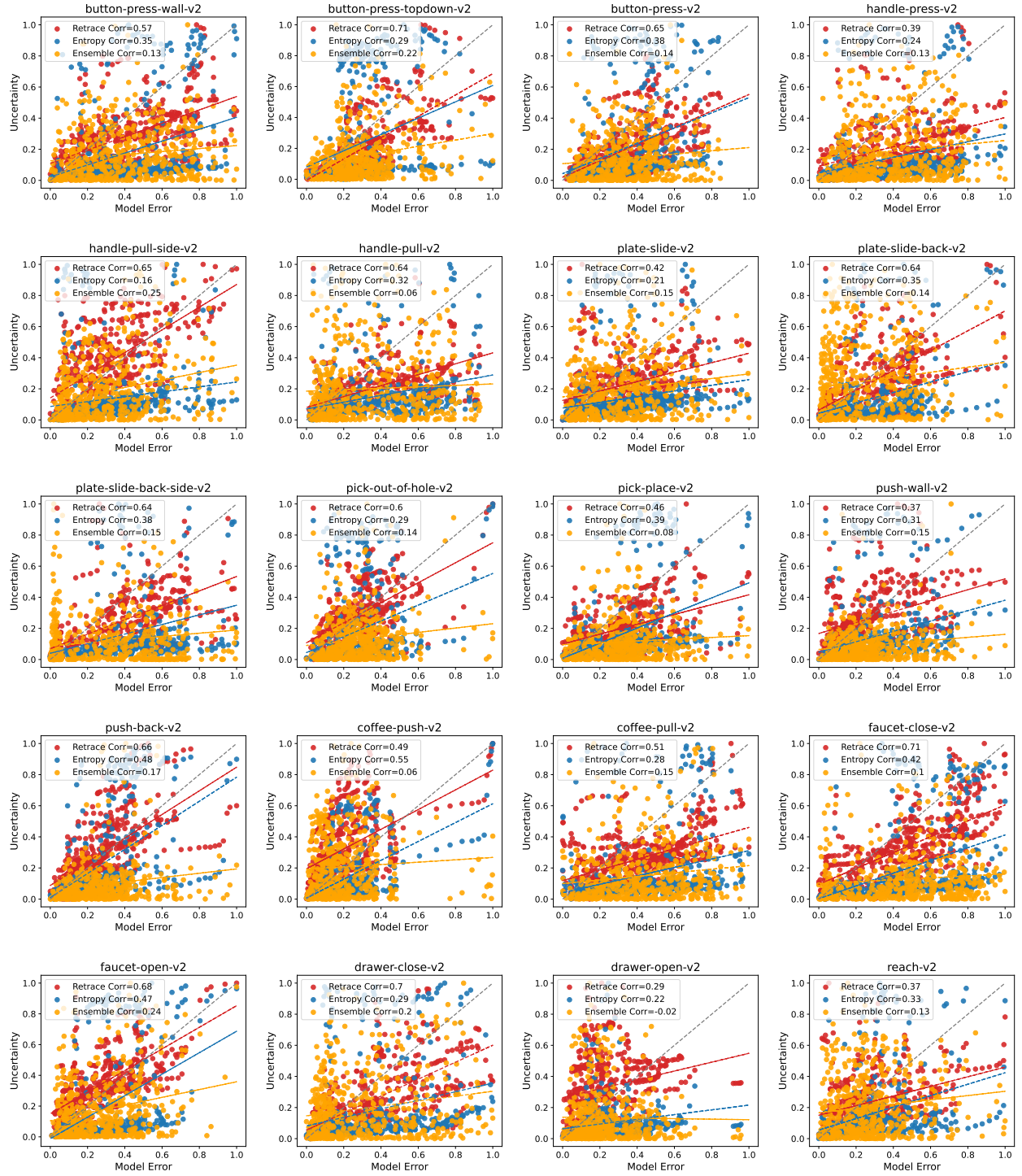


Figure 16: The correlation between the estimated uncertainty and the perceptual model error.



User

Here are two images. The first image is the last frame of a real scene, and I will provide you with another image predicted by a model. You need to determine if the two images are consistent based on **the following criteria**: 1) You can see the inside of the trash bin. 2) The ball should be simply missing and not in the desk. 3) Is there any severe distortion in the predicted image? 4) Is the position of the robotic arm in the predicted image not far away from that of the real image? When all these criterias are satisfied, we call the predicted image is consistent with the real one. Now I will show you the real image.



Please provide the predicted image so I can compare it with the real one based on the criteria you provided.



GPT-4o



User

Now I will show you the predicted image. Yes means the predicted image is consistent with the real image. No means the opposite. Just answer **yes or no** and give your reason.



Yes, the predicted image is consistent with the real image.
Reason: 1. You can see the inside of the trash bin. 2. The ball is simply missing and not in the desk. 3. There is no severe distortion in the predicted image. 4. The position of the robotic arm in the predicted image is not far away from that of the real image.



GPT-4o

Figure 17: The illustration of a Q&A example using GPT-4o for evaluating the world model's consistency rate.

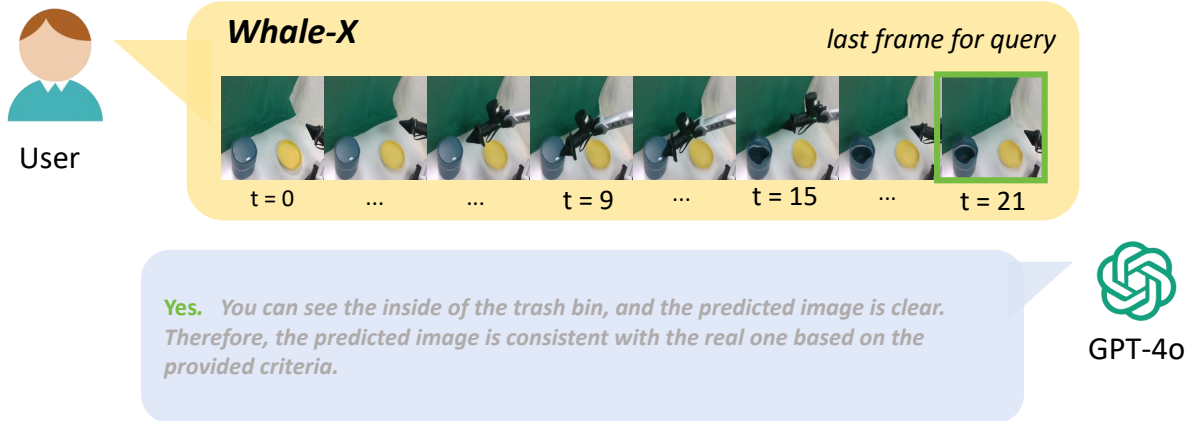


Figure 18: The example of GPT-4o evaluation for Whale-X on the Visual Generalization Task.

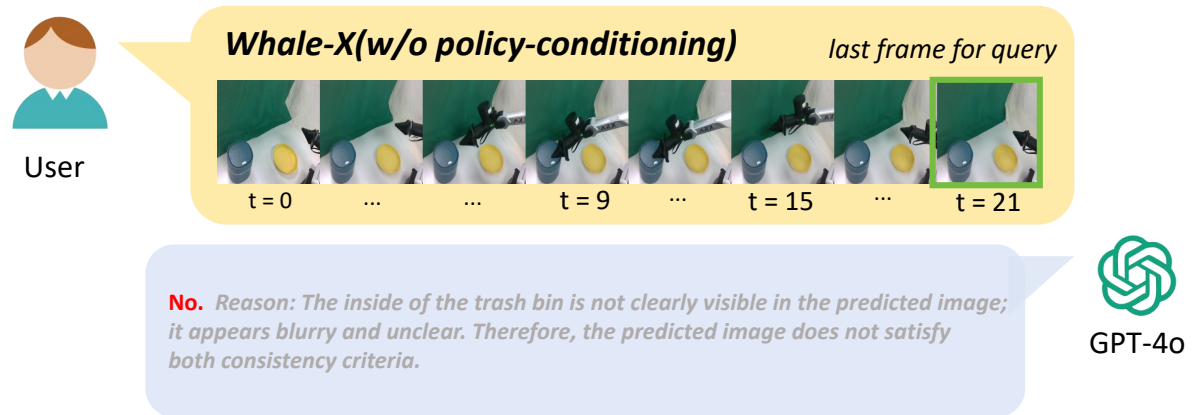


Figure 19: The example of GPT-4o evaluation for Whale-X(w/o policy-conditioning) on the Visual Generalization Task.

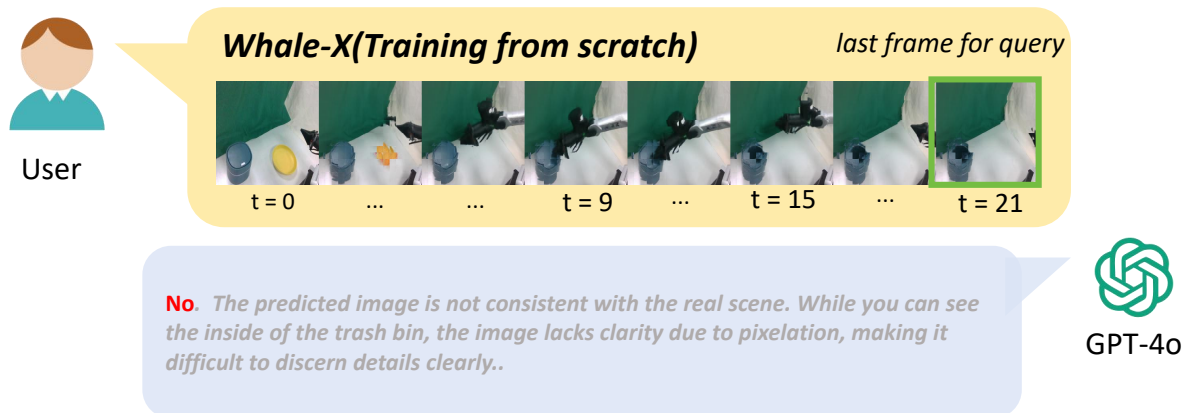


Figure 20: The example of GPT-4o evaluation for Whale-X(Training from scratch) on the Visual Generalization Task.

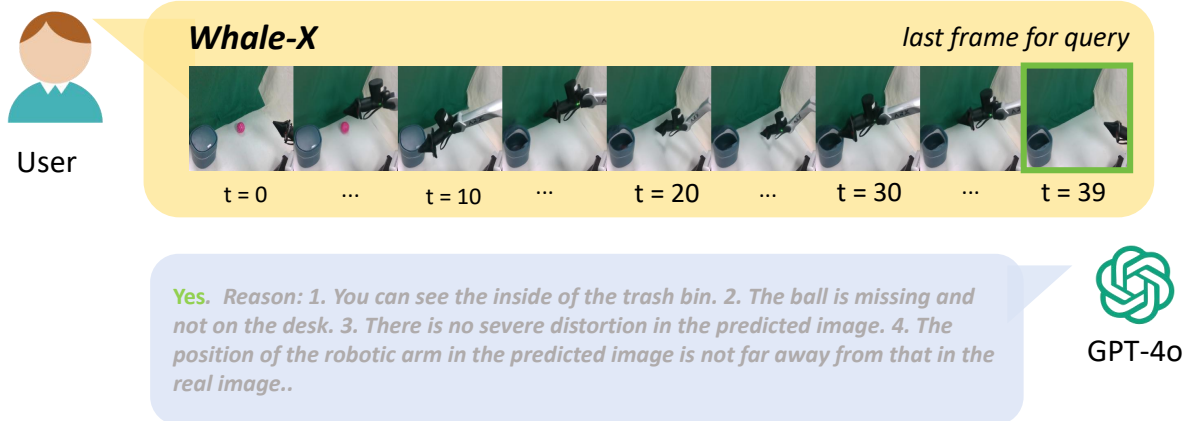


Figure 21: The example of GPT-4o evaluation for Whale-X on the Task Generalization Task.

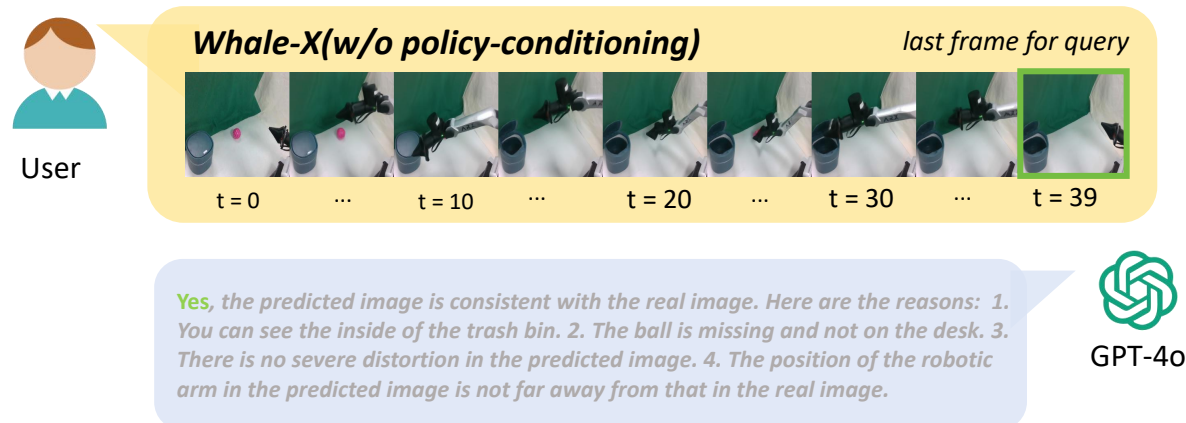


Figure 22: The example of GPT-4o evaluation for Whale-X(w/o policy-conditioning) on the Task Generalization Task.

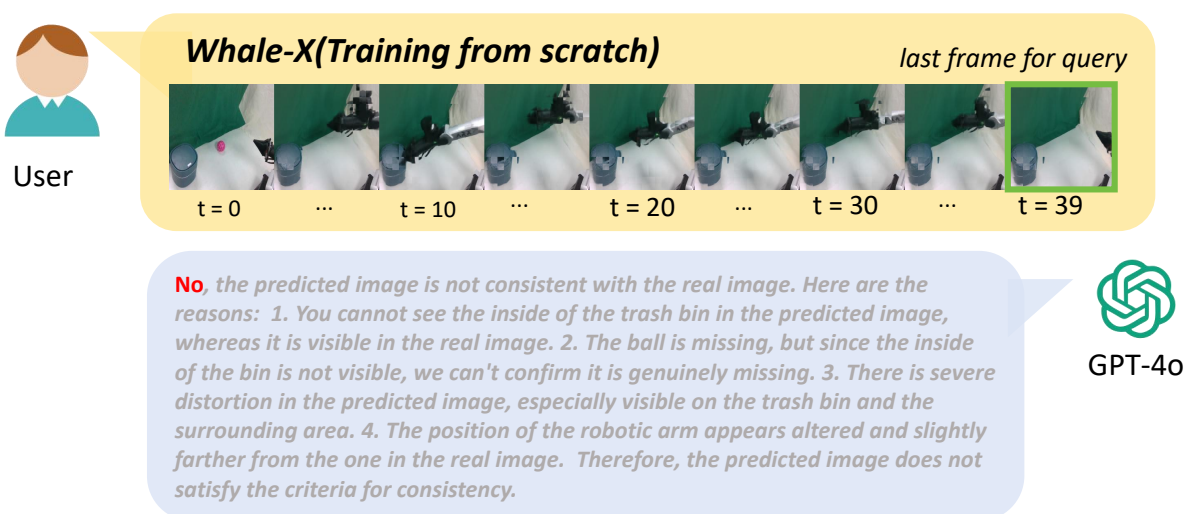


Figure 23: The example of GPT-4o evaluation for Whale-X(Training from scratch) on the Task Generalization Task.

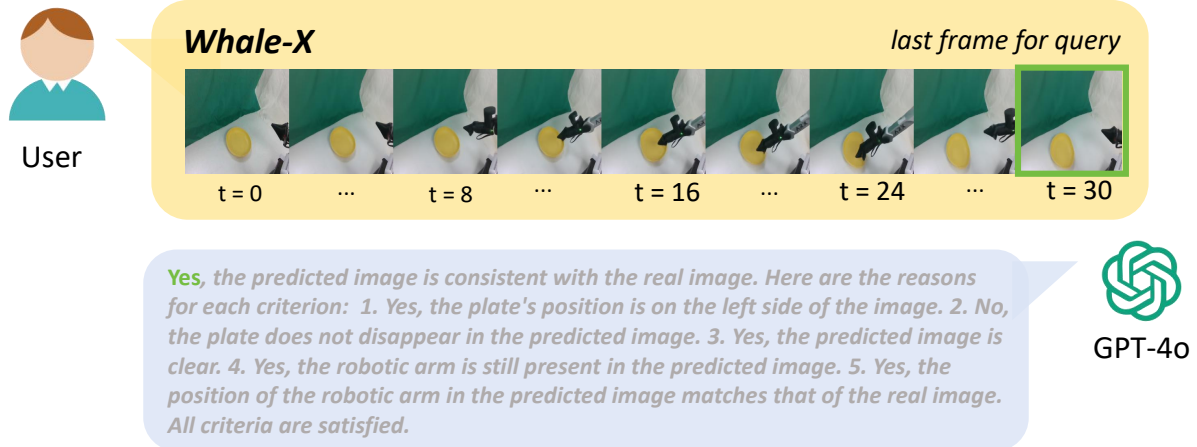


Figure 24: The example of GPT-4o evaluation for Whale-X on the Motion Generalization Task.

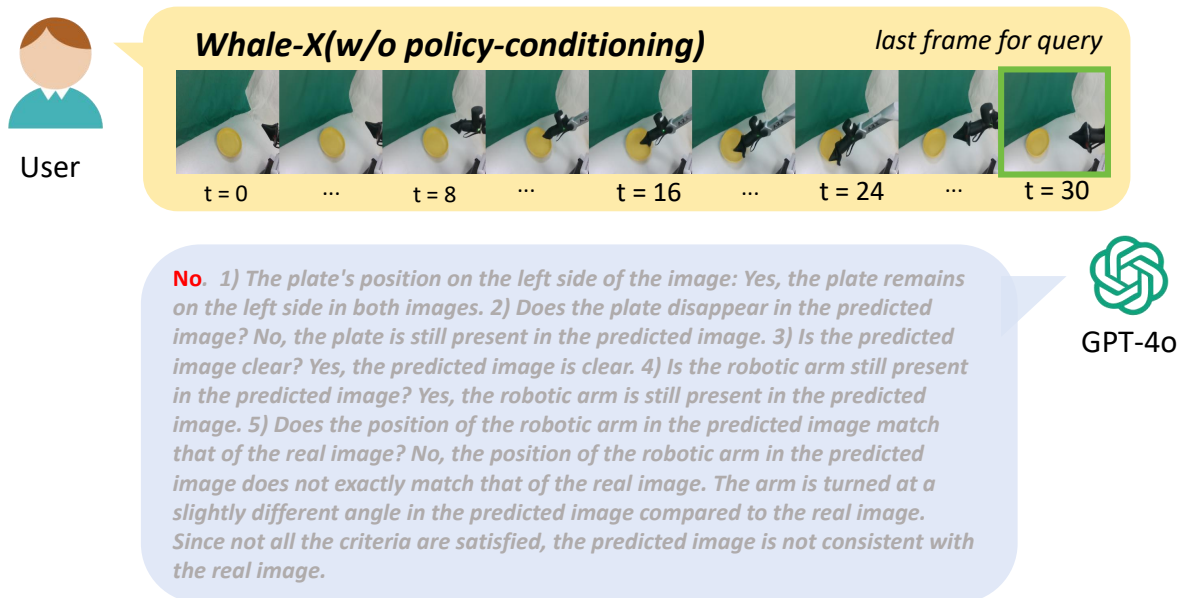


Figure 25: The example of GPT-4o evaluation for Whale-X(w/o policy-conditioning) on the Motion Generalization Task.

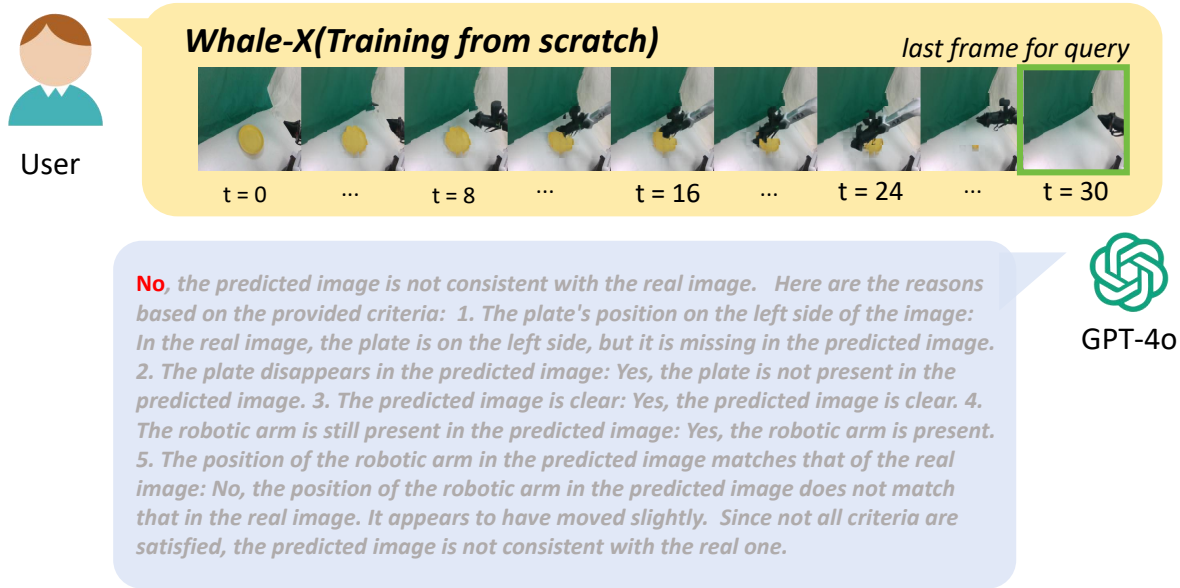


Figure 26: The example of GPT-4o evaluation for Whale-X(Training from scratch) on the Motion Generalization Task.